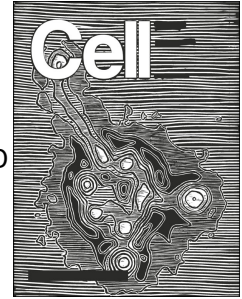


# Journal Pre-proof



SARS-CoV-2 mRNA vaccination induces functionally diverse antibodies to NTD, RBD and S2

Fatima Amanat, Mahima Thapa, Tinting Lei, Shaza M. Sayed Ahmed, Daniel C. Adelsberg, Juan Manuel Carreno, Shirin Strohmeier, Aaron J. Schmitz, Sarah Zafar, Julian Q. Zhou, Willemijn Rijnink, Hala Alshammary, Nicholas Borchering, Ana Gonzalez Reiche, Komal Srivastava, Emilia Mia Sordillo, Harm van Bakel, The Personalized Virology Initiative, Jackson S. Turner, Goran Bajic, Viviana Simon, Ali H. Ellebedy, Florian Krammer

PII: S0092-8674(21)00706-6

DOI: <https://doi.org/10.1016/j.cell.2021.06.005>

Reference: CELL 12079

To appear in: *Cell*

Received Date: 9 March 2021

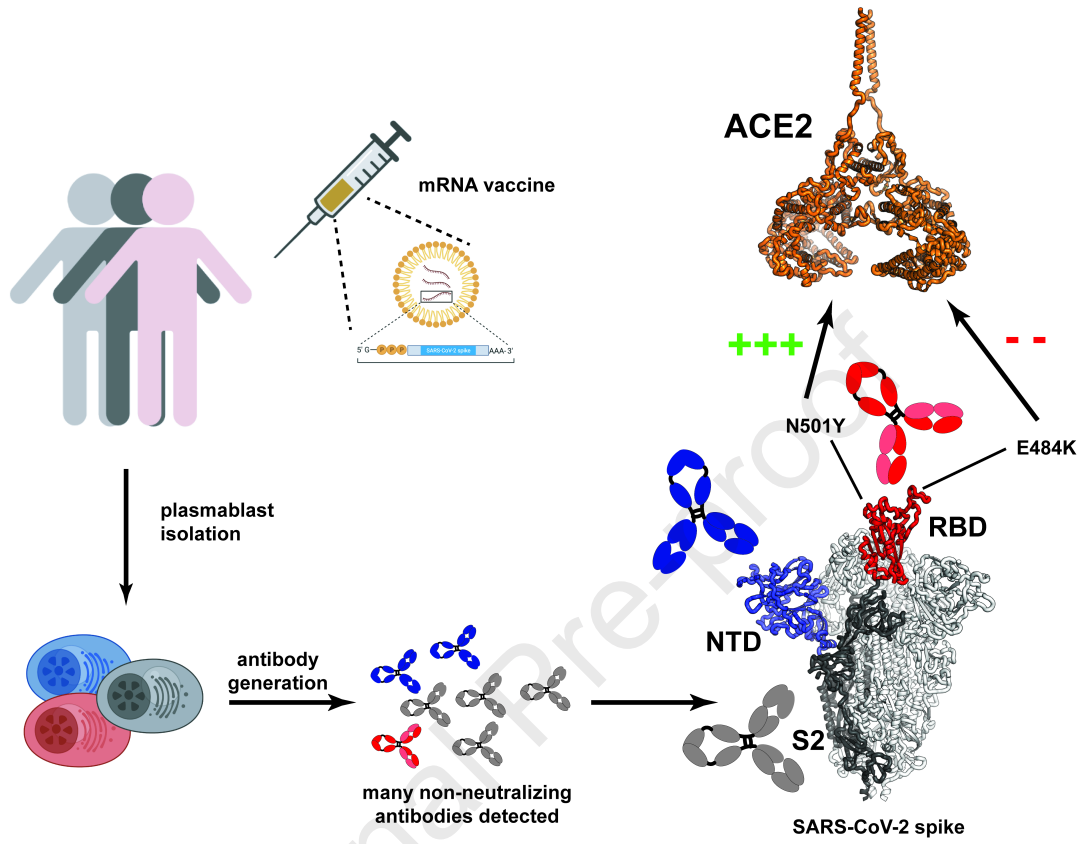
Revised Date: 14 May 2021

Accepted Date: 2 June 2021

Please cite this article as: Amanat, F., Thapa, M., Lei, T., Sayed Ahmed, S.M., Adelsberg, D.C., Carreno, J.M., Strohmeier, S., Schmitz, A.J., Zafar, S., Zhou, J.Q., Rijnink, W., Alshammary, H., Borchering, N., Reiche, A.G., Srivastava, K., Sordillo, E.M., van Bakel, H., The Personalized Virology Initiative, Turner, J.S., Bajic, G., Simon, V., Ellebedy, A.H., Krammer, F., SARS-CoV-2 mRNA vaccination induces functionally diverse antibodies to NTD, RBD and S2, *Cell* (2021), doi: <https://doi.org/10.1016/j.cell.2021.06.005>.

This is a PDF file of an article that has undergone enhancements after acceptance, such as the addition of a cover page and metadata, and formatting for readability, but it is not yet the definitive version of record. This version will undergo additional copyediting, typesetting and review before it is published in its final form, but we are providing this version to give early visibility of the article. Please note that, during the production process, errors may be discovered which could affect the content, and all legal disclaimers that apply to the journal pertain.

© 2021 Published by Elsevier Inc.



1 **SARS-CoV-2 mRNA vaccination induces functionally diverse antibodies to NTD, RBD and S2**

2

3 Fatima Amanat<sup>1,2</sup>, Mahima Thapa<sup>3</sup>, Tinting Lei<sup>3</sup>, Shaza M. Sayed Ahmed<sup>3</sup>, Daniel C. Adelsberg<sup>1</sup>, Juan  
 4 Manuel Carreno<sup>1</sup>, Shirin Strohmeier<sup>1</sup>, Aaron J. Schmitz<sup>3</sup>, Sarah Zafar<sup>1</sup>, Julian Q Zhou<sup>4</sup>, Willemijn Rijnink<sup>1</sup>,  
 5 Hala Alshammary<sup>1</sup>, Nicholas Borchering<sup>3</sup>, Ana Gonzalez Reiche<sup>5</sup>, Komal Srivastava, Emilia Mia Sordillo<sup>6</sup>,  
 6 Harm van Bakel<sup>5,7</sup>, The Personalized Virology Initiative<sup>#</sup>, Jackson S. Turner<sup>3</sup>, Goran Bajic<sup>1</sup>, Viviana  
 7 Simon<sup>1,8,9</sup>, Ali H. Ellebedy<sup>3,10,11</sup>, Florian Krammer<sup>1,12</sup>

8 *Affiliations*

9 <sup>1</sup>*Department of Microbiology, Icahn School of Medicine at Mount Sinai, New York, NY 10029, USA*

10 <sup>2</sup>*Graduate School of Biomedical Sciences, Icahn School of Medicine at Mount Sinai, New York, NY 10029,*  
 11 *USA*

12 <sup>3</sup>*Department of Pathology & Immunology, Washington University School of Medicine, St. Louis, MO,*  
 13 *63110, USA*

14 <sup>4</sup>*AbCellera Biologics Inc., Vancouver, BC V5Y 0A1, Canada*

15 <sup>5</sup>*Department of Genetics and Genomic Sciences, Icahn School of Medicine at Mount Sinai, New York, NY*  
 16 *10029, USA*

17 <sup>6</sup>*Department of Pathology, Molecular and Cell Based Medicine, Icahn School of Medicine at Mount Sinai,*  
 18 *New York, NY 10029, USA*

19 <sup>7</sup>*Icahn Institute for Data Science and Genomic Technology, Icahn School of Medicine at Mount Sinai,*  
 20 *New York, NY 10029, USA*

21 <sup>8</sup>*Division of Infectious Diseases, Department of Medicine, Icahn School of Medicine at Mount Sinai, New*  
 22 *York, NY 10029, USA*

23 <sup>9</sup>*The Global Health and Emerging Pathogens Institute, Icahn School of Medicine at Mount Sinai, New*  
 24 *York, NY 10029, USA*

25 <sup>10</sup>*Andrew M. and Jane M. Bursky Center for Human Immunology and Immunotherapy Programs,*  
 26 *Washington University School of Medicine, Saint Louis, MO 63110, USA*

27 <sup>11</sup>*Center for Vaccines and Immunity to Microbial Pathogens, Washington University School of Medicine,*  
 28 *Saint Louis, MO 63110, USA*

29 <sup>12</sup>*Lead Contact*

30

31 <sup>#</sup>*Personalized Virology Initiative (PVI) Study group/Consortium (in alphabetical order): Dr. Bulbul Ahmed,*  
 32 *Dr. Deena Altman, Angela Amoako, Mahmoud Awawda, Katherine Beach, Carolina Bermúdez-González,*  
 33 *Rachel Chernet, Lily Eaker, Shelcie Fabre, Emily. D. Ferreri, Daniel Floda, Charles Gleason, Dr. Giulio*  
 34 *Kleiner, Dr. Denise Jurczynszak, Julia Matthews, Wannu Mendez, Dr. Lubbertus CF Mulder, Jose Polanco,*  
 35 *Kayla Russo, Ashley Salimbangon, Dr. Miti Saksena, Amber S. Shin , Levy Sominsky, Sayahi Suthakaran,*  
 36 *Dr. Ania Wajnberg*

37

38 **Corresponding authors**

39 Goran Bajic, goran.bajic@mssm.edu

40 Viviana Simon, viviana.simon@mssm.edu

41 Ali H. Ellebedy, ellebedy@wustl.edu

42 Florian Krammer, florian.krammer@mssm.edu

43 **Summary**

44 In this study we profiled vaccine-induced polyclonal antibodies as well as plasmablast derived mAbs  
45 from individuals who received SARS-CoV-2 spike mRNA vaccine. Polyclonal antibody responses in  
46 vaccinees were robust and comparable to or exceeded those seen after natural infection. However, the  
47 ratio of binding to neutralizing antibodies after vaccination was greater than that after natural infection  
48 and, at the monoclonal level, we found that the majority of vaccine-induced antibodies did not have  
49 neutralizing activity. We also found a co-dominance of mAbs targeting the NTD and RBD of SARS-CoV-2  
50 spike and an original antigenic-sin like backboost to seasonal human coronaviruses OC43 and HKU1.  
51 Neutralizing activity of NTD mAbs but not RBD mAbs against a clinical viral isolate carrying E484K as well  
52 as extensive changes in the NTD was abolished, suggesting that a proportion of vaccine induced RBD  
53 binding antibodies may provide substantial protection against viral variants carrying single E484K RBD  
54 mutations.

55

56

57

58

59

60

61

62

63

64

65 **Introduction**

66 Understanding of the innate and adaptive immune responses to severe acute respiratory  
67 syndrome coronavirus 2 (SARS-CoV-2) has progressed rapidly since the beginning of the coronavirus  
68 disease 2019 (COVID-19) pandemic (Carvalho et al., 2021). Polyclonal antibody responses against the  
69 spike protein of the virus in serum, and to a lesser degree also at mucosal surfaces, have been well  
70 characterized with respect to their kinetics, binding capacity and functionality (Grandjean et al., 2020;  
71 Isho et al., 2020; Iyer et al., 2020; Ripperger et al., 2020; Seow et al., 2020; Wajnberg et al., 2020).  
72 Similarly, encouraging data have been published on both the plasmablast response and the memory B-  
73 cell response induced by SARS-CoV-2 infection (Dan et al., 2021; Gaebler et al., 2020; Guthmiller et al.,  
74 2021; Huang et al., 2021; Robbiani et al., 2020; Rodda et al., 2021; Wilson et al., 2020). The immune  
75 responses to SARS-CoV-2 vaccination, including to mRNA-based vaccines, are less well studied since  
76 these vaccines have only become available in the last months of 2020 (Baden et al., 2020; Polack et al.,  
77 2020). However, understanding vaccine-induced immunity is of high importance given the goal to  
78 achieve immunity for most people through vaccination, rather than as a consequence of infection.

79 The receptor binding domain (RBD) of the SARS-CoV-2 spike is an important target for  
80 serological and B-cell studies because it directly interacts with the cellular receptor angiotensin  
81 converting enzyme 2 (ACE2) mediating host cell entry (Letko et al., 2020; Wrapp et al., 2020). Antibodies  
82 binding to the RBD can potently block attachment of the virus to ACE2 and thereby neutralize the virus  
83 (Barnes et al., 2020). As a consequence, RBD-based vaccines are in development in addition to full  
84 length spike-based vaccines (Krammer, 2020). Analyses of the B-cell responses to the spike generally  
85 focus on the RBD and on cells sorted with RBD baits introducing an inherent bias by omitting non-RBD  
86 targets (Cao et al., 2020; Gaebler *et al.*, 2020; Robbiani *et al.*, 2020; Weisblum et al., 2020). This is also  
87 true for B cells and monoclonal antibodies (mAbs) isolated from vaccinated individuals (Wang et al.,  
88 2021). However, other epitopes within the spike protein, notably the N-terminal domain (NTD) but also  
89 S2, do harbor neutralizing epitopes (Chi et al., 2020; Liu et al., 2020; McCallum et al., 2021b; Song et al.,  
90 2020). In fact, the NTD is heavily mutated in the three most prominent variants of concern (VOCs,  
91 B.1.1.7, B.1.351 and P.1 (Davies et al., 2021; Faria et al., 2021; Tegally et al., 2020)). Here, we studied the  
92 unbiased plasmablast response to SARS-CoV-2 mRNA-based vaccination and report several new findings.  
93 First, we document that RBD and NTD co-dominate as B-cell targets on the viral spike protein,  
94 highlighting the importance of the NTD. We also report the first vaccine-induced NTD mAbs. In addition,  
95 we show that the majority of mAbs isolated are non-neutralizing, which is reflective of the higher  
96 binding to neutralization ratios found in serum after vaccination compared to natural infection. Finally,  
97 data from plasmablasts suggest that, at least, some of the vaccine-induced response is biased by pre-  
98 existing immunity to human  $\beta$ -coronaviruses.

99

## 100 Results

### 101 **The polyclonal antibody response to mRNA vaccination exceeds titers seen in convalescent individuals** 102 **but is characterized by a high ratio of non-neutralizing antibodies**

103 In late 2020, six adult participants of an ongoing observational study received mRNA-based  
104 SARS-CoV-2 vaccines (**Suppl. Table 1**). Blood from these individuals (termed V1-V6) was collected at  
105 several time points including before vaccination (for 4/6), after the first vaccination and at several time  
106 points after the second vaccination. We examined their immune responses to recombinant spike protein  
107 and RBD in enzyme-linked immunosorbent assays (ELISA), in comparison to those of 30 COVID-19  
108 survivors (**Figure 1A and 1B, Suppl. Table 1**). The sera from convalescent individuals were selected  
109 based on their anti-spike titers and grouped into three groups (low +: n=8; moderate ++: n=11; and high  
110 +++: n=11, based on the antibody titer measured in the Mount Sinai's CLIA laboratory (Wajnberg *et al.*,  
111 2020), taken 111-273 days post symptom onset), in order to facilitate identifying different features that  
112 may track with the strength of the antibody response. Five out of six vaccinees produced anti-spike and  
113 anti-RBD responses that were, at the peak, markedly higher than responses observed even in the high  
114 titer convalescent group while one vaccinee (V4) produced titers comparable to the high titer group.  
115 Notably, the antibody response peaked one week after the second vaccine dose, followed by a decline  
116 in titers over the following weeks as expected from an antibody response to vaccination. Interestingly,  
117 anti-RBD antibody titers seemed to decline faster than anti-spike antibody titers, which appeared to be  
118 more stable over time. We also measured neutralizing antibody titers using authentic SARS-CoV-2 and  
119 found a similar trend with all vaccinees displaying high titers, even though V4 responded with delayed  
120 kinetics (**Figure 1C**). Importantly, although at the peak response, the vaccine group mounted  
121 neutralization titers that fell in the upper range for the high convalescent group, they did not exceed  
122 that group markedly. This finding prompted us to calculate the proportions of spike binding to  
123 neutralizing antibodies. For the convalescent group, we found that individuals with lower titers had a  
124 higher proportion of binding to neutralizing antibodies than high responding convalescent individuals  
125 (**Figure 1D**). When determined at the time of peak response, the vaccinees had the highest proportion  
126 of binding to neutralizing antibody titers, indicating an immune response focused on non-neutralizing  
127 antibodies or an induction of less potent neutralizing antibodies in general (or both). These proportions  
128 remained stable over time with the ratio of binding to neutralizing antibodies in vaccinated individuals  
129 being significantly higher than those observed for any of the three convalescent groups ( $p = 0.0004$ ,  
130  $0.0002$  and  $0.0041$  for the three groups respectively; **Suppl. Figure 1**). We also investigated the spike  
131 binding to RBD binding ratio and found no difference to convalescent individuals except a general trend  
132 towards proportionally less RBD binding over time in the vaccinees (**Suppl. Figure 1**).

### 133 **mRNA vaccination induces a modest but measurable immune response to seasonal $\beta$ -coronavirus** 134 **spike proteins**

135 It has been reported that SARS-CoV-2 infection induces an original antigenic sin-type immune  
136 response against human coronaviruses (hCoVs) to which the majority of the human population has pre-  
137 existing immunity (Aydillo *et al.*, 2020; Song *et al.*, 2020). Here, we explored whether this phenomenon  
138 is also induced by SARS-CoV-2 mRNA vaccination. Antibody titers in four vaccinees against spike protein  
139 from  $\alpha$ -coronaviruses 229E and NL63 were detectable at the pre-vaccination time point, but did not  
140 increase substantially post-vaccination (**Figure 1E-F**; for V5 and V6 no pre-vaccination serum was  
141 available). However, titers against the spike proteins of  $\beta$ -coronaviruses OC43 and HKU1 increased

142 substantially in these four vaccinees after vaccination (**Figure 1G-H**). Thus, vaccination with mRNA SARS-  
143 CoV-2 spike also boosts immune responses against seasonal  $\beta$ -coronavirus spike proteins in a manner  
144 reminiscent of that reported for natural infection with SARS-CoV-2.

#### 145 **Plasmablast response to SARS-CoV-2 mRNA vaccination targets both the RBD and the NTD**

146 In order to characterize the B-cell response to vaccination in an unbiased manner, plasmablasts  
147 were single-cell sorted from blood specimens obtained from three individuals (V3, V5 and V6) one week  
148 after the booster immunization (**Suppl. Figure 2**). All mAbs were generated from single-cell sorted  
149 plasmablasts and probed for binding to recombinant SARS-CoV-2 spike protein. Twenty-one (40 mAbs  
150 were screened, with 28 being clonally unique, **Suppl. Table 2**) spike-reactive mAbs were isolated from  
151 V3, six (82 screened, 20 unique) from V5 and fifteen (84 screened, 24 unique) from V6 (**Figure 2A**). Using  
152 recombinant spike, RBD, NTD and S2 proteins, we mapped the domains to which these mAbs bind.  
153 Interestingly, only a minority of these antibodies recognized RBD (24% for V3, 47% for V6 and no RBD  
154 binders were identified for V5) (**Figure 2B and 2E**). A substantial number of the isolated mAbs bound to  
155 NTD including 14% for V3, 33% for V5 and 33% for V6 (**Figure 2C and 2E**). These data indicate that RBD  
156 and NTD are co-dominant in the context of mRNA-induced plasmablast response. The epitopes for the  
157 majority of the remaining spike binding mAbs, 52% for V3, 50% for V5 and 20% for V6, mapped to S2  
158 (**Figure 2D and 2E**). Only three mAbs were not accounted for in terms of binding target (two for V3 and  
159 one for V5, **Figure 2E**).

#### 160 **The majority of isolated mAbs from SARS-CoV2 vaccinees are non-neutralizing**

161 All antibodies were tested for neutralizing activity against the USA-WA1/2020 strain of SARS-  
162 CoV-2. Only a minority of the binding antibodies, even those targeting the RBD, showed neutralizing  
163 activity (**Figure 2F and 2G**). For V3, only one (an RBD binder) out of 21 mAbs (5%) displayed neutralizing  
164 activity (**Figure 2G**). For V5, a single NTD antibody neutralized authentic SARS-CoV-2 (17%) (**Figure 2G**).  
165 The highest frequency of neutralizing antibodies was found in V6 (34%) with one RBD neutralizer and  
166 four NTD neutralizers (**Figure 2G**). Interestingly, the highest neutralizing potency was found in mAb  
167 PVI.V5-6, an NTD binder followed by PVI.V6-4, an RBD binder.

168 We also tested all the antibodies for reactivity to the spike proteins of the four hCoVs 229E,  
169 NL63, HKU1 and OC43. No antibody binding to the spike proteins of  $\alpha$ -coronaviruses 229E and NL63 was  
170 found but we identified five mAbs (including three from V3, one from V5 and one from V6) that bound,  
171 to varying degrees, to the spike of OC43, which, like SARS-CoV-2, is a  $\beta$ -coronavirus (**Figure 2H**). Three  
172 mAbs showed strong binding (PVI.V3-8, PVI.V3-12 and PVI.V6-1), while PVI.V3-17 showed an  
173 intermediate binding phenotype and PVI.V5-1 bound very weakly. Three of these mAbs also showed  
174 binding to the spike of HKU1, another  $\beta$ -coronavirus. Of these, PVI.V6-1 showed only very weak binding  
175 while PVI.V3-8 and PVI.V3-12 had low minimal binding concentrations (MBCs) indicating higher affinity  
176 (**Figure 2I**).

#### 177 **The spike-reactive plasmablast response is dominated by IgG1+ cells and is comprised of a mixture of 178 cells with low and high levels of somatic hypermutation (SHM)**

179 Single-cell RNA sequencing (scRNAseq) was performed on bulk sorted plasmablasts from the  
180 three vaccinees (V3, V5, V6) to comprehensively examine the transcriptional profile, isotype distribution  
181 and somatic hypermutation (SHM) of vaccine-induced plasmablasts. We analyzed 4,584, 3,523 and

182 4,461 single cells from subjects V3, V5, and V6, respectively. We first verified the identity of sequenced  
183 cells as plasmablasts through the combined expression of B cell receptors (BCRs) (**Figure 3A**) and that of  
184 the canonical transcription as well as other factors essential for plasma cell differentiation, such as  
185 *PRDM1*, *XBP1* and *MZB1* (**Figure 3B**). To identify vaccine-responding B cell clones among the analyzed  
186 plasmablasts, we used scRNAseq to also analyze gene expression and V(D)J libraries from the sorted  
187 plasmablasts and clonally matched the BCR sequences to those from which spike-specific mAbs had  
188 been made. Using this method, we recovered 332, 7 and 1,384 BCR sequences from the scRNAseq data  
189 that are clonally related to the spike-binding mAbs derived from subjects V3, V5 and V6, respectively  
190 (**Figure 3C**). It is important to note here that we were not able to recover clonally related sequences for  
191 all of the mAbs that we cloned and expressed from each of the three vaccinees.

192 We next examined the isotype and IgG subclass distribution among the recovered sequences.  
193 IgG1 was by far the most dominant isotype in the three vaccinees (**Figure 3D**). Finally, we assessed the  
194 level of somatic hypermutation (SHM) among the mAbs-related sequences from the three subjects. We  
195 used the SHM levels observed in human naïve B cells and seasonal influenza virus vaccination-induced  
196 plasmablasts that were previously published for comparison (Turner et al., 2020). Spike-reactive  
197 plasmablasts from V3 and V6 but not V5 had accumulated SHM at levels that are significantly greater  
198 than those observed with naïve B cells (**Figure 3E, left panel**). Strikingly, the SHM among V6  
199 plasmablasts was equivalent to those observed after seasonal influenza virus vaccination (**Figure 3E, left  
200 panel**). We reasoned that the high level of SHM among spike-reactive plasmablasts may be derived from  
201 those targeting conserved epitopes that are shared with human  $\beta$ -coronaviruses. Indeed, we found that  
202 the SHM level among clones that are related to cross-reactive mAbs was significantly higher than their  
203 non-cross-reactive counterparts (**Figure 3E, right panel**).

#### 204 **Competition of RBD binding neutralizing mAbs with ACE2 and affinity of variant RBDs for human ACE2**

205 Two mAbs were identified as neutralizing and binding to RBD. We wanted, therefore, to test if  
206 they competed with ACE2 for RBD binding. Concentration-dependent competition was indeed observed  
207 for both mAbs demonstrating that inhibition of ACE2 binding is the mechanism of action of the two  
208 mAbs (**Figure 4**). Since we prepared RBD proteins of viral variants of concern for analysis of antibody  
209 binding (see below), we also wanted to assess the affinity of each variant RBD for human ACE2. Using  
210 biolayer interferometry (BLI), we measured association and dissociation rates of the N501Y RBD mutant  
211 (B.1.1.7 carries that mutation as its sole RBD mutation), Y453F, as found in mink isolates (Larsen et al.,  
212 2021), N439K, which is found in some European clades (Thomson et al., 2021), a combination of Y453F  
213 and N439K, E484K (part of B.1.351 and P.1) as well as for the B.1.351 and the P.1 RBDs for a  
214 recombinant version of human ACE2 (**Figure 4A, 4B and 4D**). Almost all of the single and double  
215 mutations in RBD tested increased affinity to human ACE2. Specifically, N501Y and Y453F combined with  
216 N439K increased affinity for human ACE2 by 5-fold (**Figure 4D, Suppl. Figure 3**). In contrast, E484K on its  
217 own decreased affinity by 4-fold. Of note, the B.1.351 RBD affinity for ACE2 was comparable to that of  
218 the wild-type RBD. These data were confirmed using an ELISA-based method which showed the same  
219 trends (**Suppl. Figure 4**).

#### 220 **Binding profiles of polyclonal serum and mAbs to RBDs carrying mutations found in viral variants of 221 concern**

222 Next, we assessed binding of sera from vaccinated individuals, COVID-19 survivors and mAbs  
223 derived from plasmablasts to variant RBDs. Our panel of RBDs includes published mAb escape mutants,

224 RBD mutants detected by the Mount Sinai Hospital's Pathogen Surveillance Program in patients seeking  
225 care at the Mount Sinai Health System in NYC as well as mutations found in viral variants of interest and  
226 variants of concern (Baum et al., 2020; Greaney et al., 2021b; Larsen *et al.*, 2021; Thomson *et al.*, 2021;  
227 Weisblum *et al.*, 2020). Serum from convalescent individuals showed strong fluctuations depending on  
228 the viral variant (**Figure 5A**). In general, single mutants E406Q, E484K and F490K exerted the biggest  
229 impact on binding. However, complete loss of binding was rare and 2-4-fold reduction in binding was  
230 more common. Interestingly, almost all sera bound better to N501Y RBD (B.1.1.7) than to wild-type RBD  
231 (average 129% compared to wild type). Conversely, the B.1.351 RBD caused, on average, a 39%  
232 reduction in binding. The impact was slightly lower for the P.1 RBD (average 70% binding compared to  
233 wild-type). For sera from the six vaccinated individuals, however, the highest reduction seen was only  
234 two-fold for E406Q, N440K, E484K and F490K (**Figure 5B**). Of note, the vaccinees' later samples (V1=d89,  
235 V2=d102, V3=d47, V4=d48, V5=49 and V6=48) were assayed to allow for some affinity maturation. The  
236 highest reduction observed for E484K, F484A, B.1.351 and P.1 were also approximately two-fold but this  
237 did not apply to all six vaccinees. Some vaccinees maintained binding levels against these RBDs at levels  
238 comparable to wild-type RBD.

239 RBD binding mAbs were also tested for binding to the same variants. In general, mAbs  
240 maintained binding levels within 2-fold of the binding seen with the wild-type RBD with some  
241 exceptions. In fact, for most mAbs, no impact on binding was observed (**Figure 5C**) with the exception of  
242 PVI.V3-9, which lost binding to the RBD carrying F486A. Although there was a negative impact on  
243 binding of several mAbs to the B.1.351 variant, binding was almost unaffected by the mutations in the  
244 P.1 variant RBD. Only one mAb, PVI.V6-4, showed a drop in binding to P.1.

#### 245 **Escape of an NTD and E484K mutant virus from polyclonal post-vaccination serum is negligible but** 246 **NTD mutations significantly impact the neutralizing activity of NTD binding mAbs**

247 Through the Mount Sinai Hospital's Pathogen Surveillance Program, we had access to the SARS-  
248 CoV-2 isolate PV14252 (Clade 20C, Pango lineage B.1) that featured two mutations (W64R, L141Y) and  
249 one deletion ( $\Delta$ 142-145) in the NTD as well as the E484K mutation in the RBD (**Figure 5D**). To determine  
250 the susceptibility of this virus variant to neutralization by post-vaccination serum, we performed  
251 microneutralization assays. Wild-type SARS-CoV-2 and PV14252 were tested in parallel to ensure that  
252 the assay setup for both viruses allowed comparison. We found a relatively minor impact when testing  
253 polyclonal sera from vaccinees for neutralizing activity (**Figure 5E**). The activity of sera from V2, V5 and  
254 V6 slightly increased while the activity for V1, V3 and V4 decreased. Next, we tested the seven  
255 neutralizing mAbs that we isolated from plasmablasts. Consistent with their binding profiles in the  
256 variant RBD ELISA, the two RBD mAbs neutralized both viruses with comparable efficiency (**Figure 5F**). In  
257 fact, the activity of PVI.V3-9 increased slightly (**Figure 5F**). In stark contrast, all five anti-NTD antibodies  
258 completely lost neutralizing activity against PV14252 due to mutations present in the NTD of this viral  
259 isolate.

#### 260 **B.1.1.7 and B.1.351 partially escape from plasmablast derived neutralizing antibodies**

261 We also tested the neutralizing activity of the two RBD and the five NTD antibodies against the  
262 variants of concern B.1.1.7 and B.1.351 (**Figure 5G**). Both variants contain deletions as well as mutations  
263 in the NTD. In addition, B.1.1.7 carries the N501Y RBD mutation and B.1.351 carries N417K, E484K and  
264 N501Y mutations in the RBD (**Figure 4 A and B**). The two RBD binding antibodies lost no (PVI.V6-4) or  
265 little (PVI.V3-9) neutralizing activity against B.1.1.7. However, PVI.V3-9 lost all activity against B.1.351

266 and the remaining neutralizing activity of PVI.V6-4 was low (but measurable). All but one (PVI.V6-11))  
267 NTD mAbs lost neutralizing activity against B.1.1.7 and all of them lost neutralizing activity against  
268 B.1.351 once more highlighting the importance of changes in the NTD on the antibody activity.

269

## 270 Discussion

271 Our knowledge of B-cell responses to SARS-CoV-2 mRNA vaccination remains incomplete. We  
272 urgently need information about the nature of polyclonal vaccine-induced responses as well as  
273 unbiased, in depth analyses of plasmablast responses. Our data provide important new insights into  
274 these responses in comparison with immune responses to natural infection. Indeed, SARS-CoV-2  
275 infection results in a very heterogeneous antibody response to the spike protein in terms of antibody  
276 quantity. In contrast, mRNA vaccination appears to induce a high antibody response of relatively  
277 homogenous titers. However, we also found that vaccinees generate more non-neutralizing antibodies  
278 than COVID-19 survivors resulting in a lower ratio of neutralizing to binding antibodies. These data were  
279 already apparent in the early phase clinical trials but remained unrecognized at the time (Walsh et al.,  
280 2020). Interestingly, low titer convalescent serum had the highest relative amount of neutralizing  
281 antibodies, whereas the proportion of binding antibodies was increased in sera with higher measured  
282 antibody titers. The majority of plasmablasts sampled after vaccination do, in fact, produce non-  
283 neutralizing antibodies. Two recent studies have performed a similarly unbiased plasmablast analysis for  
284 individuals naturally infected with SARS-CoV-2 (Cho et al., 2021; Huang *et al.*, 2021). Of course, the  
285 antibody response after SARS-CoV-2 infection is not only targeting the spike protein but several other  
286 proteins expressed by the virus. When accounting for spike binding only, these studies report  
287 proportions of 44% and 25% neutralizing antibodies (Cho *et al.*, 2021; Huang *et al.*, 2021). While  
288 plasmablast analysis is in general not quantitative (e.g. one clone per clonotype is selected etc.) our  
289 analysis of post-vaccination plasmablasts found a lower number of neutralizing antibodies (17%).

290 Future studies are needed to reveal the role of non-neutralizing antibodies in SARS-CoV-2  
291 immune protection. Indeed, antibody functions other than neutralization have been shown to correlate  
292 with protection (Bartsch et al., 2021; Gorman et al., 2021; Schäfer et al., 2021). The importance of  
293 absolute antibody titers and not ratios is underscored by the fact that post-vaccination neutralization  
294 titers were equal to or exceeded the titers found in the high responder convalescent group.

295 Of the four seasonal CoVs that are widely circulating in humans,  $\beta$ -coronaviruses OC43 and HKU1 have  
296 higher homology to SARS-CoV-2 spike. Vaccinated individuals mounted a response to spike proteins  
297 from OC43 and HKU1 but not to  $\alpha$ -coronaviruses 229E and NL63. This phenomenon resembles the  
298 immune imprinting described in influenza virus immunology and has already been shown for natural  
299 infection with SARS-CoV-2 where a 'backboost' to  $\beta$ -coronaviruses was also found (Aydillo *et al.*, 2020;  
300 Song *et al.*, 2020). A few of the mAbs isolated in our study had, indeed, such a cross-reactive phenotype.  
301 It remains unclear whether these antibodies, which target mostly S2 epitopes, contribute to protection  
302 against SARS-CoV-2, OC43 or HKU1 infection. However, the cross-reactive epitopes of mAbs that do bind  
303 SARS-CoV-2, HKU1 and OC43 spikes could provide the basis for future pan- $\beta$ -coronavirus vaccines. While  
304 it is likely the case that the B-cells producing these mAbs come from recall responses and were initially  
305 induced by human  $\beta$ -coronaviruses (which is supported by serology and of course the extensive SHM  
306 that the mAbs show), they could hypothetically also be *de novo* induced antibodies. While this is  
307 probably not the case, we cannot exclude this possibility with our current data.

308  
309 Another interesting point we noted is the co-dominance of RBD and NTD. Previous analyses of  
310 B-cell responses to SARS-CoV-2 mRNA vaccination focused on cells baited by labeled RBD (Wang *et al.*,  
311 2021). We, in contrast, took an unbiased approach to sort and clone plasmablasts in an antigen-agnostic  
312 manner. We found similar levels of NTD and RBD binders with many mAbs binding to epitopes outside  
313 the RBD and the NTD. In one vaccinee not a single RBD binding mAbs was isolated with the caveats that  
314 the overall number of mAbs derived from that individual were low and their polyclonal serum antibody  
315 responses included RBD recognition. These data suggest that the NTD, which also harbors neutralizing  
316 epitopes, is - at least - as important as the RBD and warrants as much attention. In fact, five out of seven  
317 neutralizing antibodies isolated in this study bound to the NTD and only two targeted the RBD. Recent  
318 studies analyzing the plasmablast response after natural infection have found a similar co-dominance of  
319 RBD and NTD (Cho *et al.*, 2021; Huang *et al.*, 2021) with one study reporting 59 mAbs targeting the RBD,  
320 64 targeting the NTD and 46 binding outside of RBD and NTD and the second study finding 10 RBD  
321 mAbs, 13 non-RBD S1 binding mAbs (strongly suggesting NTD binding) and 9 mAbs targeting S2.  
322 Interestingly, and in contrast to our findings, a recent deep mutational scanning paper with sera from  
323 mRNA-1273 found a very strong RBD-focused response (Greaney *et al.*, 2021a). Further characterization  
324 of the mAbs obtained in our study showed a complete loss of neutralization against an authentic,  
325 replication-competent variant virus that harbored extensive changes in the NTD. All NTD mAbs also lost  
326 neutralizing activity against B.1.351 and all but one lost activity against B.1.1.7. These observations may  
327 explain why a reduction in neutralization against the viral variant of concern B.1.1.7 is seen in some  
328 studies despite the fact the N501Y substitution in the RBD of this variant does not significantly impact  
329 binding and neutralizing activity (Emary *et al.*, 2021). The key role of NTD as target for antibodies has  
330 recently also been shown using memory B cell derived mAbs (McCallum *et al.*, 2021a).

331 In addition, we assessed the impact of different RBD mutations on affinity towards human ACE2.  
332 Interestingly, N501Y increased the affinity by five-fold. This increase in receptor binding affinity may  
333 contribute to the higher infectivity of B.1.1.7, which carries this mutation in its RBD. In contrast,  
334 introduction of E484K reduced the affinity by 4-fold which may explain why virus variants carrying only  
335 the E484K mutation have rarely spread efficiently, although viruses carrying E484K have been detected  
336 since the fall of 2020 in a handful of patients receiving care at the Mount Sinai Health System and have  
337 also been reported in immunocompromised patients (Choi *et al.*, 2020). It is tempting to speculate that  
338 the N501Y mutation enables the acquisition of E484K without a fitness loss. In fact, the B.1.351 RBD,  
339 which carries N501Y and E484K (as well as N417K) showed binding to hACE2 that was similar to wild-  
340 type RBD. Recently, B.1.1.7 variant strains carrying E484K, in addition to N501Y, have been isolated in  
341 the UK (PHE, 2021), providing evidence for the hypothesis that N501Y enables acquisition of mutations  
342 in the RBD that may be detrimental to receptor binding. However, recent expansion of B.1.526, a  
343 lineage also featuring E484K but without N501Y in New York City, suggests that this fitness loss may be  
344 overcome by other, yet uncharacterized, changes in the virus as well (Annavaiahala *et al.*, 2021; Lasek-  
345 Nesselquist *et al.*, 2021). Interestingly, binding of convalescent sera to the N501Y RBD was also  
346 increased, suggesting that changes that increase affinity for the receptor may also increase affinity of a  
347 set of antibodies that may mimic the receptor.

348 We also noted that the two neutralizing antibodies against the RBD showed some reduced  
349 binding to a mutant RBD carrying the E484K mutation while having similar or even increased neutralizing  
350 potency against a variant virus carrying the E484K mutation as the only change in its RBD. The reduced

351 affinity of the E484K variant RBD for hACE2 could render the virus more susceptible to RBD binding  
352 mAbs. Thus, an antibody binding to the RBD may just be more effective in interfering with a low affinity  
353 as compared to a high affinity RBD-hACE2 interaction. Increased affinity as an escape mechanism for  
354 viruses has been described in the past (Hensley et al., 2009; O'Donnell et al., 2012) and the converse  
355 mechanism could be at play here.

356 Whether or not the current vaccines will provide effective protection against circulating and  
357 emerging viral variants of concern is an important question which has gathered a lot of attention in early  
358 2021. Our data indicate that reduction in binding to the E484K and B.1.351 variant RBDs was minor  
359 (often only 2-fold) compared to reported reduction in neutralization (which ranges from 6-8 fold to  
360 complete loss of neutralization (Cele et al., 2021; Wibmer et al., 2021; Wu et al., 2021)). Although not  
361 tested here, it is likely that the reduction in binding to full length spike is even lower, given the many  
362 epitopes on the spike other than NTD and RBD. The maintenance of binding to a large degree observed  
363 in this study suggests that viral variants will have a minor impact on serological assays which are  
364 currently in wide use for medical, scientific and public health reasons. Binding, non-neutralizing  
365 antibodies have also been shown to have a protective effect in many viral infections (Asthagiri  
366 Arunkumar et al., 2019; Dilillo et al., 2014; Saphire et al., 2018) and may be a factor in the substantial  
367 residual protection seen in the Johnson & Johnson and Novavax vaccine trials against B.1.351 in South  
368 Africa (Shinde et al., 2021). Production of non-neutralizing antibodies may also play a role in protection  
369 by mRNA vaccines after the first dose, as it is substantial and occurs during a time when neutralizing  
370 antibody titers are either very low or absent (Baden *et al.*, 2020; Dagan et al., 2021; Polack *et al.*, 2020).  
371 Finally, although some antibodies may lose neutralizing activity due to reduced affinity, they do still  
372 bind. Furthermore, B cells with these specificities potentially could undergo affinity maturation after  
373 exposure to a variant virus or a variant spike-containing vaccine, leading to high affinity antibodies to  
374 variant viruses of concern.

375 In summary, we demonstrate that the antibody responses to SARS-CoV-2 mRNA vaccination comprise a  
376 large proportion of non-neutralizing antibodies and are co-dominated by NTD and RBD antibodies. The  
377 NTD portion of the spike represents, thus, an important vaccine target. Since all viral variants of concern  
378 are heavily mutated in this region, these observations warrant further attention to optimize SARS-CoV-2  
379 vaccines. Finally, broadly cross-reactive mAbs to  $\beta$ -coronavirus spike proteins are induced after  
380 vaccination, and suggest a potential development path for a pan-  $\beta$ -coronavirus vaccine.

### 381 **Limitations of the Study**

382 While our study characterizes the antibody response after SARS-CoV-2 mRNA vaccination in detail, it has  
383 several limitations. The first limitation is the small number of study participants, which makes this study  
384 a qualitative rather than a quantitative study. Another limitation is the lack of plasmablast analysis of  
385 SARS-CoV-2 infected individuals. We have compared our data with published data from plasmablast  
386 analysis after SARS-CoV-2 infection but a side-by-side comparison would have been more accurate. We  
387 have also not included a longitudinal analysis of the convalescent sera in the study but feel that  
388 providing a wide range of time points and titer levels offsets this limitation to a certain degree. In  
389 addition, while the clones of crossreactive plasmablasts are likely derived from the memory  
390 compartment and have likely been initially induced by seasonal coronavirus infections, we lack the  
391 ultimate proof for that since we did not analyze pre-vaccination memory B cells and B cell receptor

392 sequences. Finally, the burning question if the abundant non-neutralizing antibodies do have a  
393 protective effect *in vivo* will need to be elucidated by follow up studies.

394

395

#### 396 **Acknowledgements**

397 We would like to thank the study participants for their generosity and willingness to participate in  
398 longitudinal COVID19 research studies. None of this work would be possible without their contributions.  
399 We would like to thank Dr. Randy A. Albrecht for oversight of the conventional BSL3 biocontainment  
400 facility, which makes our work with live SARS-CoV-2 possible. We are also grateful for Mount Sinai's  
401 leadership during the COVID-19 pandemic. We want to especially thank Drs. Peter Palese, Carlos  
402 Cordon-Cardo, Dennis Charney, David Reich and Kenneth Davis for their support. We would also like to  
403 thank Bassem Mohamed and Wooseob Kim for their help with preparing the scRNAseq libraries. This  
404 work was partially funded by the NIAID Collaborative Influenza Vaccine Innovation Centers (CIVIC)  
405 contract 75N93019C00051, NIAID Center of Excellence for Influenza Research and Surveillance (CEIRS,  
406 contract # HHSN272201400008C and HHSN272201400006C), NIAID grants U01AI141990 and  
407 U01AI150747, by the generous support of the JPB Foundation and the Open Philanthropy Project  
408 (research grant 2020-215611 (5384); and by anonymous donors. J.S.T. was supported by NIAID  
409 5T32CA009547.

410

#### 411 **Conflict of interest statement**

412 The Icahn School of Medicine at Mount Sinai has filed patent applications relating to SARS-CoV-2  
413 serological assays and NDV-based SARS-CoV-2 vaccines which list Florian Krammer as co-inventor.  
414 Viviana Simon is also listed on the serological assay patent application as co-inventors. Mount Sinai has  
415 spun out a company, Kantaro, to market serological tests for SARS-CoV-2. Florian Krammer has  
416 consulted for Merck and Pfizer (before 2020), and is currently consulting for Pfizer, Seqirus and Avimex.  
417 The Krammer laboratory is also collaborating with Pfizer on animal models of SARS-CoV-2. Ali Ellebedy  
418 has consulted for InBios and Fimbrion Therapeutics (before 2021) and is currently a consultant for  
419 Mubadala Investment Company. The Ellebedy laboratory received funding under sponsored research  
420 agreements that are unrelated to the data presented in the current study from Emergent BioSolutions  
421 and from AbbVie.

422

#### 423 **Author contributions**

424 FA, GB, VS, AHE and FK developed the concept. HA, KS, PVI and VS recruited patients and performed  
425 clinical coordination. MT, TL, SMSA, AJS, NB and JST performed the antibody isolation. JQZ and AHE  
426 performed the B-cell sequence analysis. AGR, HvB and EMS acquired samples and sequenced viruses.  
427 FA, JMC, SS, SZ and WR characterized sera and mAbs and created reagents. DCA measured affinities. FA,  
428 GB, VS, AHE and FK analyzed the data. GB, VS, AHE and FK created the figures. FK wrote the manuscript.  
429 FA, GB, VS and AHE edited the manuscript. All authors read, subedited and approved the manuscript.

430

431

432 **References**

- 433 Amanat, F., Duehr, J., Huang, C., Paessler, S., Tan, G.S., and Krammer, F. (2020a). Monoclonal Antibodies  
 434 with Neutralizing Activity and Fc-Effector Functions against the Machupo Virus Glycoprotein. *J Virol* *94*.  
 435 10.1128/JVI.01741-19.
- 436 Amanat, F., Duehr, J., Oestereich, L., Hastie, K.M., Ollmann Saphire, E., and Krammer, F. (2018).  
 437 Antibodies to the Glycoprotein GP2 Subunit Cross-React between Old and New World Arenaviruses.  
 438 *mSphere* *3*. 10.1128/mSphere.00189-18.
- 439 Amanat, F., Stadlbauer, D., Strohmeier, S., Nguyen, T.H.O., Chromikova, V., McMahon, M., Jiang, K.,  
 440 Arunkumar, G.A., Jurczynszak, D., Polanco, J., et al. (2020b). A serological assay to detect SARS-CoV-2  
 441 seroconversion in humans. *Nat Med* *26*, 1033-1036. 10.1038/s41591-020-0913-5.
- 442 Amanat, F., White, K.M., Miorin, L., Strohmeier, S., McMahon, M., Meade, P., Liu, W.C., Albrecht, R.A.,  
 443 Simon, V., Martinez-Sobrido, L., et al. (2020c). An In Vitro Microneutralization Assay for SARS-CoV-2  
 444 Serology and Drug Screening. *Curr Protoc Microbiol* *58*, e108. 10.1002/cpmc.108.
- 445 Annavajhala, M.K., Mohri, H., Zucker, J.E., Sheng, Z., Wang, P., Gomez-Simmonds, A., Ho, D.D., and  
 446 Uhlemann, A.C. (2021). A Novel SARS-CoV-2 Variant of Concern, B.1.526, Identified in New York.  
 447 *medRxiv*. 10.1101/2021.02.23.21252259.
- 448 Asthagiri Arunkumar, G., Ioannou, A., Wohlbold, T.J., Meade, P., Aslam, S., Amanat, F., Ayllon, J., García-  
 449 Sastre, A., and Krammer, F. (2019). Broadly Cross-Reactive, Nonneutralizing Antibodies against Influenza  
 450 B Virus Hemagglutinin Demonstrate Effector Function-Dependent Protection against Lethal Viral  
 451 Challenge in Mice. *J Virol* *93*. 10.1128/JVI.01696-18.
- 452 Aydilto, T., Rombauts, A., Stadlbauer, D., Aslam, S., Abelenda-Alonso, G., Escalera, A., Amanat, F., Jiang,  
 453 K., Krammer, F., Carratala, J., and García-Sastre, A. (2020). Antibody Immunological Imprinting on  
 454 COVID-19 Patients. *medRxiv*, 2020.2010.2014.20212662. 10.1101/2020.10.14.20212662.
- 455 Baden, L.R., El Sahly, H.M., Essink, B., Kotloff, K., Frey, S., Novak, R., Diemert, D., Spector, S.A., Roupheal,  
 456 N., Creech, C.B., et al. (2020). Efficacy and Safety of the mRNA-1273 SARS-CoV-2 Vaccine. *N Engl J Med*.  
 457 10.1056/NEJMoa2035389.
- 458 Bailey, M.J., Broecker, F., Duehr, J., Arumemi, F., Krammer, F., Palese, P., and Tan, G.S. (2019).  
 459 Antibodies Elicited by an NS1-Based Vaccine Protect Mice against Zika Virus. *mBio* *10*.  
 460 10.1128/mBio.02861-18.
- 461 Barnes, C.O., West, A.P., Huey-Tubman, K.E., Hoffmann, M.A.G., Sharaf, N.G., Hoffman, P.R., Koranda,  
 462 N., Gristick, H.B., Gaebler, C., Muecksch, F., et al. (2020). Structures of Human Antibodies Bound to  
 463 SARS-CoV-2 Spike Reveal Common Epitopes and Recurrent Features of Antibodies. *Cell* *182*, 828-  
 464 842.e816. 10.1016/j.cell.2020.06.025.
- 465 Bartsch, Y.C., Fischinger, S., Siddiqui, S.M., Chen, Z., Yu, J., Gebre, M., Atyeo, C., Gorman, M.J., Zhu, A.L.,  
 466 Kang, J., et al. (2021). Discrete SARS-CoV-2 antibody titers track with functional humoral stability. *Nat*  
 467 *Commun* *12*, 1018. 10.1038/s41467-021-21336-8.
- 468 Baum, A., Fulton, B.O., Wloga, E., Copin, R., Pascal, K.E., Russo, V., Giordano, S., Lanza, K., Negron, N., Ni,  
 469 M., et al. (2020). Antibody cocktail to SARS-CoV-2 spike protein prevents rapid mutational escape seen  
 470 with individual antibodies. *Science* *369*, 1014-1018. 10.1126/science.abd0831.
- 471 Borchering, N., Bormann, N.L., and Kraus, G. (2020). scRepertoire: An R-based toolkit for single-cell  
 472 immune receptor analysis. *F1000Res* *9*, 47. 10.12688/f1000research.22139.2.
- 473 Cao, Y., Su, B., Guo, X., Sun, W., Deng, Y., Bao, L., Zhu, Q., Zhang, X., Zheng, Y., Geng, C., et al. (2020).  
 474 Potent Neutralizing Antibodies against SARS-CoV-2 Identified by High-Throughput Single-Cell Sequencing  
 475 of Convalescent Patients' B Cells. *Cell* *182*, 73-84.e16. 10.1016/j.cell.2020.05.025.
- 476 Carvalho, T., Krammer, F., and Iwasaki, A. (2021). The first 12 months of COVID-19: a timeline of  
 477 immunological insights. *Nat Rev Immunol* *21*, 245-256. 10.1038/s41577-021-00522-1.

478 Cele, S., Gazy, I., Jackson, L., Hwa, S.-H., Tegally, H., Lustig, G., Giandhari, J., Pillay, S., Wilkinson, E.,  
479 Naidoo, Y., et al. (2021). Escape of SARS-CoV-2 501Y.V2 variants from neutralization by convalescent  
480 plasma. medRxiv, 2021.2001.2026.21250224. 10.1101/2021.01.26.21250224.

481 Chi, X., Yan, R., Zhang, J., Zhang, G., Zhang, Y., Hao, M., Zhang, Z., Fan, P., Dong, Y., Yang, Y., et al. (2020).  
482 A neutralizing human antibody binds to the N-terminal domain of the Spike protein of SARS-CoV-2.  
483 *Science* 369, 650-655. 10.1126/science.abc6952.

484 Cho, H., Gonzales-Wartz, K.K., Huang, D., Yuan, M., Peterson, M., Liang, J., Beutler, N., Torres, J.L., Cong,  
485 Y., Postnikova, E., et al. (2021). Ultrapotent bispecific antibodies neutralize emerging SARS-CoV-2  
486 variants. bioRxiv, 2021.2004.2001.437942. 10.1101/2021.04.01.437942.

487 Choi, B., Choudhary, M.C., Regan, J., Sparks, J.A., Padera, R.F., Qiu, X., Solomon, I.H., Kuo, H.H., Boucau,  
488 J., Bowman, K., et al. (2020). Persistence and Evolution of SARS-CoV-2 in an Immunocompromised Host.  
489 *N Engl J Med* 383, 2291-2293. 10.1056/NEJMc2031364.

490 Dagan, N., Barda, N., Kepten, E., Miron, O., Perchik, S., Katz, M.A., Hernán, M.A., Lipsitch, M., Reis, B.,  
491 and Balicer, R.D. (2021). BNT162b2 mRNA Covid-19 Vaccine in a Nationwide Mass Vaccination Setting. *N*  
492 *Engl J Med*. 10.1056/NEJMoa2101765.

493 Dan, J.M., Mateus, J., Kato, Y., Hastie, K.M., Yu, E.D., Faliti, C.E., Grifoni, A., Ramirez, S.I., Haupt, S.,  
494 Frazier, A., et al. (2021). Immunological memory to SARS-CoV-2 assessed for up to 8 months after  
495 infection. *Science* 371. 10.1126/science.abf4063.

496 Davies, N.G., Abbott, S., Barnard, R.C., Jarvis, C.I., Kucharski, A.J., Munday, J.D., Pearson, C.A.B., Russell,  
497 T.W., Tully, D.C., Washburne, A.D., et al. (2021). Estimated transmissibility and impact of SARS-CoV-2  
498 lineage B.1.1.7 in England. *Science*, eabg3055. 10.1126/science.abg3055.

499 Dilillo, D.J., Tan, G.S., Palese, P., and Ravetch, J.V. (2014). Broadly neutralizing hemagglutinin stalk-  
500 specific antibodies require FcγR interactions for protection against influenza virus in vivo. *Nat Med*.  
501 10.1038/nm.3443.

502 Emary, K.R.W., Golubchik, T., Aley, P.K., Ariani, C.V., Angus, B., Bibi, S., Blane, B., Bonsall, D., Cicconi, P.,  
503 Charlton, S., et al. (2021). Efficacy of ChAdOx1 nCoV-19 (AZD1222) vaccine against SARS-CoV-2 variant of  
504 concern 202012/01 (B.1.1.7): an exploratory analysis of a randomised controlled trial. *Lancet* 397, 1351-  
505 1362. 10.1016/S0140-6736(21)00628-0.

506 Faria, N.R., Claro, I.M., Candido, D., Franco, L.A.M., Andrade, P.S., Coletti, T.M., Silva, C.A.M., Sales, F.C.,  
507 Manula, E.R., Aguiar, R.S., et al. (2021). `<h1 data-topic-id="586" style="font-size: 1.7511em; margin: 0px  
508 0px 4px; font-family: Helvetica, Arial, sans-serif; width: 999px; line-height: 1.2; overflow-wrap: break-  
509 word; color: rgb(34, 34, 34); background-color: rgb(255, 255, 255);">Genomic characterisation of an  
510 emergent SARS-CoV-2 lineage in Manaus: preliminary findings.`

511 Gaebler, C., Wang, Z., Lorenzi, J.C.C., Muecksch, F., Finkin, S., Tokuyama, M., Ladinsky, M., Cho, A.,  
512 Jankovic, M., Schaefer-Babajew, D., et al. (2020). Evolution of Antibody Immunity to SARS-CoV-2.  
513 bioRxiv. 10.1101/2020.11.03.367391.

514 Giudicelli, V., Chaume, D., and Lefranc, M.P. (2005). IMGT/GENE-DB: a comprehensive database for  
515 human and mouse immunoglobulin and T cell receptor genes. *Nucleic Acids Res* 33, D256-261.  
516 10.1093/nar/gki010.

517 Gonzalez-Reiche, A.S., Hernandez, M.M., Sullivan, M.J., Ciferri, B., Alshammery, H., Obla, A., Fabre, S.,  
518 Kleiner, G., Polanco, J., Khan, Z., et al. (2020). Introductions and early spread of SARS-CoV-2 in the New  
519 York City area. *Science*. 10.1126/science.abc1917.

520 Gorman, M.J., Patel, N., Guebre-Xabier, M., Zhu, A., Atyeo, C., Pullen, K.M., Loos, C., Goez-Gazi, Y.,  
521 Carrion, R., Tian, J.-H., et al. (2021). Collaboration between the Fab and Fc contribute to maximal  
522 protection against SARS-CoV-2 in nonhuman primates following NVX-CoV2373 subunit vaccine with  
523 Matrix-M™ vaccination. bioRxiv, 2021.2002.2005.429759. 10.1101/2021.02.05.429759.

524 Grandjean, L., Saso, A., Torres, A., Lam, T., Hatcher, J., Thistlethwayte, R., Harris, M., Best, T., Johnson,  
525 M., Wagstaffe, H., et al. (2020). Humoral Response Dynamics Following Infection with SARS-CoV-2.  
526 medRxiv, 2020.2007.2016.20155663. 10.1101/2020.07.16.20155663.

527 Greaney, A.J., Loes, A.N., Gentles, L.E., Crawford, K.H.D., Starr, T.N., Malone, K.D., Chu, H.Y., and Bloom,  
528 J.D. (2021a). The SARS-CoV-2 mRNA-1273 vaccine elicits more RBD-focused neutralization, but with  
529 broader antibody binding within the RBD. bioRxiv, 2021.2004.2014.439844.  
530 10.1101/2021.04.14.439844.

531 Greaney, A.J., Starr, T.N., Gilchuk, P., Zost, S.J., Binshtein, E., Loes, A.N., Hilton, S.K., Huddleston, J.,  
532 Eguia, R., Crawford, K.H.D., et al. (2021b). Complete Mapping of Mutations to the SARS-CoV-2 Spike  
533 Receptor-Binding Domain that Escape Antibody Recognition. *Cell Host Microbe* 29, 44-57.e49.  
534 10.1016/j.chom.2020.11.007.

535 Gupta, N.T., Vander Heiden, J.A., Uduman, M., Gadala-Maria, D., Yaari, G., and Kleinstein, S.H. (2015).  
536 Change-O: a toolkit for analyzing large-scale B cell immunoglobulin repertoire sequencing data.  
537 *Bioinformatics* 31, 3356-3358. 10.1093/bioinformatics/btv359.

538 Guthmiller, J.J., Stovicek, O., Wang, J., Changrob, S., Li, L., Halfmann, P., Zheng, N.Y., Utset, H., Stamper,  
539 C.T., Dugan, H.L., et al. (2021). SARS-CoV-2 Infection Severity Is Linked to Superior Humoral Immunity  
540 against the Spike. *mBio* 12. 10.1128/mBio.02940-20.

541 Hensley, S.E., Das, S.R., Bailey, A.L., Schmidt, L.M., Hickman, H.D., Jayaraman, A., Viswanathan, K.,  
542 Raman, R., Sasisekharan, R., Bennink, J.R., and Yewdell, J.W. (2009). Hemagglutinin receptor binding  
543 avidity drives influenza A virus antigenic drift. *Science* 326, 734-736. 10.1126/science.1178258.

544 Huang, K.A., Tan, T.K., Chen, T.H., Huang, C.G., Harvey, R., Hussain, S., Chen, C.P., Harding, A., Gilbert-  
545 Jaramillo, J., Liu, X., et al. (2021). Breadth and function of antibody response to acute SARS-CoV-2  
546 infection in humans. *PLoS Pathog* 17, e1009352. 10.1371/journal.ppat.1009352.

547 Isho, B., Abe, K.T., Zuo, M., Jamal, A.J., Rathod, B., Wang, J.H., Li, Z., Chao, G., Rojas, O.L., Bang, Y.M., et  
548 al. (2020). Persistence of serum and saliva antibody responses to SARS-CoV-2 spike antigens in COVID-19  
549 patients. *Sci Immunol* 5. 10.1126/sciimmunol.abe5511.

550 Iyer, A.S., Jones, F.K., Nodoushani, A., Kelly, M., Becker, M., Slater, D., Mills, R., Teng, E., Kamruzzaman,  
551 M., Garcia-Beltran, W.F., et al. (2020). Dynamics and significance of the antibody response to SARS-CoV-  
552 2 infection. medRxiv. 10.1101/2020.07.18.20155374.

553 Krammer, F. (2020). SARS-CoV-2 vaccines in development. *Nature* 586, 516-527. 10.1038/s41586-020-  
554 2798-3.

555 Lan, J., Ge, J., Yu, J., Shan, S., Zhou, H., Fan, S., Zhang, Q., Shi, X., Wang, Q., Zhang, L., and Wang, X.  
556 (2020). Structure of the SARS-CoV-2 spike receptor-binding domain bound to the ACE2 receptor. *Nature*  
557 581, 215-220. 10.1038/s41586-020-2180-5.

558 Larsen, H.D., Fonager, J., Lomholt, F.K., Dalby, T., Benedetti, G., Kristensen, B., Urth, T.R., Rasmussen, M.,  
559 Lassaunière, R., Rasmussen, T.B., et al. (2021). Preliminary report of an outbreak of SARS-CoV-2 in mink  
560 and mink farmers associated with community spread, Denmark, June to November 2020. *Euro Surveill*  
561 26. 10.2807/1560-7917.ES.2021.26.5.210009.

562 Lasek-Nesselquist, E., Lapierre, P., Schneider, E., George, K.S., and Pata, J. (2021). The localized rise of a  
563 B.1.526 SARS-CoV-2 variant containing an E484K mutation in New York State. medRxiv,  
564 2021.2002.2026.21251868. 10.1101/2021.02.26.21251868.

565 Letko, M., Marzi, A., and Munster, V. (2020). Functional assessment of cell entry and receptor usage for  
566 SARS-CoV-2 and other lineage B betacoronaviruses. *Nat Microbiol* 5, 562-569. 10.1038/s41564-020-  
567 0688-y.

568 Liu, L., Wang, P., Nair, M.S., Yu, J., Rapp, M., Wang, Q., Luo, Y., Chan, J.F., Sahi, V., Figueroa, A., et al.  
569 (2020). Potent neutralizing antibodies against multiple epitopes on SARS-CoV-2 spike. *Nature* 584, 450-  
570 456. 10.1038/s41586-020-2571-7.

571 Margine, I., Palese, P., and Krammer, F. (2013). Expression of functional recombinant hemagglutinin and  
572 neuraminidase proteins from the novel H7N9 influenza virus using the baculovirus expression system. *J*  
573 *Vis Exp*, e51112. 10.3791/51112.

574 McCallum, M., De Marco, A., Lempp, F.A., Tortorici, M.A., Pinto, D., Walls, A.C., Beltramello, M., Chen,  
575 A., Liu, Z., Zatta, F., et al. (2021a). N-terminal domain antigenic mapping reveals a site of vulnerability for  
576 SARS-CoV-2. *Cell*. 10.1016/j.cell.2021.03.028.

577 McCallum, M., Marco, A., Lempp, F., Tortorici, M.A., Pinto, D., Walls, A.C., Beltramello, M., Chen, A., Liu,  
578 Z., Zatta, F., et al. (2021b). N-terminal domain antigenic mapping reveals a site of vulnerability for SARS-  
579 CoV-2. *bioRxiv*. 10.1101/2021.01.14.426475.

580 Nachbagauer, R., Shore, D., Yang, H., Johnson, S.K., Gabbard, J.D., Tompkins, S.M., Wrammert, J.,  
581 Wilson, P.C., Stevens, J., Ahmed, R., et al. (2018). Broadly Reactive Human Monoclonal Antibodies  
582 Elicited following Pandemic H1N1 Influenza Virus Exposure Protect Mice against Highly Pathogenic H5N1  
583 Challenge. *J Virol* 92. 10.1128/JVI.00949-18.

584 O'Donnell, C.D., Vogel, L., Wright, A., Das, S.R., Wrammert, J., Li, G.M., McCausland, M., Zheng, N.Y.,  
585 Yewdell, J.W., Ahmed, R., et al. (2012). Antibody pressure by a human monoclonal antibody targeting  
586 the 2009 pandemic H1N1 virus hemagglutinin drives the emergence of a virus with increased virulence  
587 in mice. *mBio* 3. 10.1128/mBio.00120-12.

588 Pallesen, J., Wang, N., Corbett, K.S., Wrapp, D., Kirchdoerfer, R.N., Turner, H.L., Cottrell, C.A., Becker,  
589 M.M., Wang, L., Shi, W., et al. (2017). Immunogenicity and structures of a rationally designed prefusion  
590 MERS-CoV spike antigen. *Proc Natl Acad Sci U S A* 114, E7348-E7357. 10.1073/pnas.1707304114.

591 PHE (2021). Investigation of novel SARS-CoV-2 variant Variant of Concern 202012/01 Technical briefing  
592 5.

593 Polack, F.P., Thomas, S.J., Kitchin, N., Absalon, J., Gurtman, A., Lockhart, S., Perez, J.L., Pérez Marc, G.,  
594 Moreira, E.D., Zerbini, C., et al. (2020). Safety and Efficacy of the BNT162b2 mRNA Covid-19 Vaccine. *N*  
595 *Engl J Med*. 10.1056/NEJMoa2034577.

596 Ripperger, T.J., Uhrlaub, J.L., Watanabe, M., Wong, R., Castaneda, Y., Pizzato, H.A., Thompson, M.R.,  
597 Bradshaw, C., Weinkauf, C.C., Bime, C., et al. (2020). Orthogonal SARS-CoV-2 Serological Assays Enable  
598 Surveillance of Low-Prevalence Communities and Reveal Durable Humoral Immunity. *Immunity* 53, 925-  
599 933.e924. 10.1016/j.immuni.2020.10.004.

600 Robbiani, D.F., Gaebler, C., Muecksch, F., Lorenzi, J.C.C., Wang, Z., Cho, A., Agudelo, M., Barnes, C.O.,  
601 Gazumyan, A., Finkin, S., et al. (2020). Convergent antibody responses to SARS-CoV-2 in convalescent  
602 individuals. *Nature* 584, 437-442. 10.1038/s41586-020-2456-9.

603 Rodda, L.B., Netland, J., Shehata, L., Pruner, K.B., Morawski, P.A., Thouvenel, C.D., Takehara, K.K.,  
604 Eggenberger, J., Hemann, E.A., Waterman, H.R., et al. (2021). Functional SARS-CoV-2-Specific Immune  
605 Memory Persists after Mild COVID-19. *Cell* 184, 169-183.e117. 10.1016/j.cell.2020.11.029.

606 Sapphire, E.O., Schendel, S.L., Fusco, M.L., Gangavarapu, K., Gunn, B.M., Wec, A.Z., Halfmann, P.J.,  
607 Brannan, J.M., Herbert, A.S., Qiu, X., et al. (2018). Systematic Analysis of Monoclonal Antibodies against  
608 Ebola Virus GP Defines Features that Contribute to Protection. *Cell* 174, 938-952.e913.  
609 10.1016/j.cell.2018.07.033.

610 Schäfer, A., Muecksch, F., Lorenzi, J.C.C., Leist, S.R., Cipolla, M., Bournazos, S., Schmidt, F., Maison, R.M.,  
611 Gazumyan, A., Martinez, D.R., et al. (2021). Antibody potency, effector function, and combinations in  
612 protection and therapy for SARS-CoV-2 infection in vivo. *J Exp Med* 218. 10.1084/jem.20201993.

613 Seow, J., Graham, C., Merrick, B., Acors, S., Pickering, S., Steel, K.J.A., Hemmings, O., O'Byrne, A.,  
614 Kouphou, N., Galao, R.P., et al. (2020). Longitudinal observation and decline of neutralizing antibody  
615 responses in the three months following SARS-CoV-2 infection in humans. *Nat Microbiol* 5, 1598-1607.  
616 10.1038/s41564-020-00813-8.

617 Shinde, V., Bhikha, S., Hossain, Z., Archary, M., Bhorat, Q., Fairlie, L., Lalloo, U., Masilela, M.L.S.,  
618 Moodley, D., Hanley, S., et al. (2021). Preliminary Efficacy of the NVX-CoV2373 Covid-19 Vaccine Against  
619 the B.1.351 Variant. *medRxiv*, 2021.2002.2025.21252477. 10.1101/2021.02.25.21252477.

620 Smith, K., Garman, L., Wrammert, J., Zheng, N.Y., Capra, J.D., Ahmed, R., and Wilson, P.C. (2009). Rapid  
621 generation of fully human monoclonal antibodies specific to a vaccinating antigen. *Nat Protoc* 4, 372-  
622 384. 10.1038/nprot.2009.3.

623 Song, G., He, W.T., Callaghan, S., Anzanello, F., Huang, D., Ricketts, J., Torres, J.L., Beutler, N., Peng, L.,  
624 Vargas, S., et al. (2020). Cross-reactive serum and memory B cell responses to spike protein in SARS-CoV-  
625 2 and endemic coronavirus infection. *bioRxiv*. 10.1101/2020.09.22.308965.

626 Stadlbauer, D., Amanat, F., Chromikova, V., Jiang, K., Strohmeier, S., Arunkumar, G.A., Tan, J., Bhavsar,  
627 D., Capuano, C., Kirkpatrick, E., et al. (2020). SARS-CoV-2 Seroconversion in Humans: A Detailed Protocol  
628 for a Serological Assay, Antigen Production, and Test Setup. *Curr Protoc Microbiol* 57, e100.  
629 10.1002/cpmc.100.

630 Stuart, T., Butler, A., Hoffman, P., Hafemeister, C., Papalexi, E., Mauck, W.M., Hao, Y., Stoeckius, M.,  
631 Smibert, P., and Satija, R. (2019). Comprehensive Integration of Single-Cell Data. *Cell* 177, 1888-  
632 1902.e1821. 10.1016/j.cell.2019.05.031.

633 Sun, W., Leist, S.R., McCroskery, S., Liu, Y., Slamani, S., Oliva, J., Amanat, F., Schafer, A., Dinnon, K.H.,  
634 3rd, Garcia-Sastre, A., et al. (2020). Newcastle disease virus (NDV) expressing the spike protein of SARS-  
635 CoV-2 as a live virus vaccine candidate. *EBioMedicine* 62, 103132. 10.1016/j.ebiom.2020.103132.

636 Tegally, H., Wilkinson, E., Giovanetti, M., Iranzadeh, A., Fonseca, V., Giandhari, J., Doolabh, D., Pillay, S.,  
637 San, E.J., Msomi, N., et al. (2020). Emergence and rapid spread of a new severe acute respiratory  
638 syndrome-related coronavirus 2 (SARS-CoV-2) lineage with multiple spike mutations in South Africa.  
639 *medRxiv*, 2020.2012.2021.20248640. 10.1101/2020.12.21.20248640.

640 Thomson, E.C., Rosen, L.E., Shepherd, J.G., Spreafico, R., da Silva Filipe, A., Wojcechowskyj, J.A., Davis,  
641 C., Piccoli, L., Pascall, D.J., Dillen, J., et al. (2021). Circulating SARS-CoV-2 spike N439K variants maintain  
642 fitness while evading antibody-mediated immunity. *Cell*. 10.1016/j.cell.2021.01.037.

643 Turner, J.S., Zhou, J.Q., Han, J., Schmitz, A.J., Rizk, A.A., Alsoussi, W.B., Lei, T., Amor, M., McIntire, K.M.,  
644 Meade, P., et al. (2020). Human germinal centres engage memory and naive B cells after influenza  
645 vaccination. *Nature* 586, 127-132. 10.1038/s41586-020-2711-0.

646 Wajnberg, A., Amanat, F., Firpo, A., Altman, D.R., Bailey, M.J., Mansour, M., McMahon, M., Meade, P.,  
647 Mendu, D.R., Muellers, K., et al. (2020). Robust neutralizing antibodies to SARS-CoV-2 infection persist  
648 for months. *Science* 370, 1227-1230. 10.1126/science.abd7728.

649 Walsh, E.E., Frenck, R., Falsey, A.R., Kitchin, N., Absalon, J., Gurtman, A., Lockhart, S., Neuzil, K., Mulligan,  
650 M.J., Bailey, R., et al. (2020). RNA-Based COVID-19 Vaccine BNT162b2 Selected for a Pivotal Efficacy  
651 Study. *medRxiv*, 2020.2008.2017.20176651. 10.1101/2020.08.17.20176651.

652 Wang, Z., Schmidt, F., Weisblum, Y., Muecksch, F., Barnes, C.O., Finkin, S., Schaefer-Babajew, D., Cipolla,  
653 M., Gaebler, C., Lieberman, J.A., et al. (2021). mRNA vaccine-elicited antibodies to SARS-CoV-2 and  
654 circulating variants. *Nature*. 10.1038/s41586-021-03324-6.

655 Weisblum, Y., Schmidt, F., Zhang, F., DaSilva, J., Poston, D., Lorenzi, J.C., Muecksch, F., Rutkowska, M.,  
656 Hoffmann, H.H., Michailidis, E., et al. (2020). Escape from neutralizing antibodies by SARS-CoV-2 spike  
657 protein variants. *Elife* 9. 10.7554/eLife.61312.

658 Wibmer, C.K., Ayres, F., Hermanus, T., Madzivhandila, M., Kgagudi, P., Lambson, B.E., Vermeulen, M.,  
659 van den Berg, K., Rossouw, T., Boswell, M., et al. (2021). SARS-CoV-2 501Y.V2 escapes neutralization by  
660 South African COVID-19 donor plasma. *bioRxiv*, 2021.2001.2018.427166. 10.1101/2021.01.18.427166.

661 Wilson, P., Stamper, C., Dugan, H., Li, L., Asby, N., Halfmann, P., Guthmiller, J., Zheng, N.Y., Huang, M.,  
662 Stovicek, O., et al. (2020). Distinct B cell subsets give rise to antigen-specific antibody responses against  
663 SARS-CoV-2. *Res Sq*. 10.21203/rs.3.rs-80476/v1.

664 Wohlbold, T.J., Chromikova, V., Tan, G.S., Meade, P., Amanat, F., Comella, P., Hirsh, A., and Krammer, F.  
 665 (2016). Hemagglutinin Stalk- and Neuraminidase-Specific Monoclonal Antibodies Protect against Lethal  
 666 H10N8 Influenza Virus Infection in Mice. *J Virol* *90*, 851-861. 10.1128/JVI.02275-15.  
 667 Wohlbold, T.J., Nachbagauer, R., Xu, H., Tan, G.S., Hirsh, A., Brokstad, K.A., Cox, R.J., Palese, P., and  
 668 Krammer, F. (2015). Vaccination with adjuvanted recombinant neuraminidase induces broad  
 669 heterologous, but not heterosubtypic, cross-protection against influenza virus infection in mice. *mBio* *6*,  
 670 e02556. 10.1128/mBio.02556-14.  
 671 Wrammert, J., Koutsonanos, D., Li, G.M., Edupuganti, S., Sui, J., Morrissey, M., McCausland, M.,  
 672 Skountzou, I., Hornig, M., Lipkin, W.I., et al. (2011). Broadly cross-reactive antibodies dominate the  
 673 human B cell response against 2009 pandemic H1N1 influenza virus infection. *J Exp Med* *208*, 181-193.  
 674 *jem.20101352* [pii]  
 675 10.1084/jem.20101352.  
 676 Wrammert, J., Smith, K., Miller, J., Langley, W.A., Kokko, K., Larsen, C., Zheng, N.Y., Mays, I., Garman, L.,  
 677 Helms, C., et al. (2008). Rapid cloning of high-affinity human monoclonal antibodies against influenza  
 678 virus. *Nature* *453*, 667-671. 10.1038/nature06890.  
 679 Wrapp, D., Wang, N., Corbett, K.S., Goldsmith, J.A., Hsieh, C.L., Abiona, O., Graham, B.S., and McLellan,  
 680 J.S. (2020). Cryo-EM structure of the 2019-nCoV spike in the prefusion conformation. *Science*.  
 681 10.1126/science.abb2507.  
 682 Wu, K., Werner, A.P., Moliva, J.I., Koch, M., Choi, A., Stewart-Jones, G.B.E., Bennett, H., Boyoglu-Barnum,  
 683 S., Shi, W., Graham, B.S., et al. (2021). mRNA-1273 vaccine induces neutralizing antibodies against spike  
 684 mutants from global SARS-CoV-2 variants. *bioRxiv*, 2021.2001.2025.427948.  
 685 10.1101/2021.01.25.427948.  
 686 Ye, J., Ma, N., Madden, T.L., and Ostell, J.M. (2013). IgBLAST: an immunoglobulin variable domain  
 687 sequence analysis tool. *Nucleic Acids Res* *41*, W34-40. 10.1093/nar/gkt382.  
 688

## 689 Figure Legends

690 **Figure 1: Antibody responses in individuals vaccinated with mRNA-based SARS-CoV-2 vaccines.**  
 691 Antibody responses of convalescent individuals and vaccinees to full length spike protein (A) and RBD  
 692 (B) as measured by ELISA and neutralizing activity of the sera of the same individuals in a  
 693 microneutralization assay against authentic SARS-CoV-2 (C). Convalescent individuals were grouped  
 694 based on their initial antibody response (measured in a CLIA laboratory) to spike protein into +, ++, and  
 695 +++. D shows ratios between binding and neutralizing antibody levels in vaccinees and convalescent  
 696 individuals. Higher ratios indicate a bias towards non-neutralizing antibodies. E, F, G and H show  
 697 antibody responses against  $\alpha$ -coronavirus 229E and NL63 and  $\beta$ -coronavirus OC43 and HKU1 spike  
 698 proteins over time. Bars represent the geometric mean, error bars represent the 95% confidence  
 699 intervals.

700

701 **Figure 2. Characterization of mAbs derived from vaccine plasmablasts.** Binding of plasmablasts derived  
 702 from three vaccinees (V3, V5 and V6) against full length spike (A), RBD (B), NTD (C) and S2 (D). E shows  
 703 the percentages of the respective antibodies per subject. F shows neutralizing activity of the mAbs  
 704 against authentic SARS-CoV-2 and the proportion of neutralizing antibodies per subject is shown in G. H  
 705 and I show reactivity of mAbs to spike protein of human  $\beta$ -coronaviruses OC43 and HKU1. MBC =  
 706 minimal binding concentration. All experiments except data shown in H and I were performed in

707 duplicates and the mean of the duplicates is shown with standard deviation. For H and I a representative  
 708 dataset from a singlet ELISA run is shown.

709

710 **Figure 3. Characterization of bulk sorted plasmablasts via single-cell RNA sequencing. (A)** Uniform  
 711 manifold approximation and projection (UMAP) of scRNAseq from bulk plasmablast with recovered BCR  
 712 sequences (purple) or unrecovered (grey). **(B)** UMAP overlay of percent of cellular population expressing  
 713 *MZB1*, *PRDM1*, and *XPB1*. Hexbin equals 80 individual cells. **(C)** UMAP overlay of BCR sequences with  
 714 confirmed spike binding activity. **(D)** Proportional composition of heavy chains genes in the spike binding  
 715 sequences broken down by sample. **(E)** Comparison of nucleotide-level mutation frequency in  
 716 immunoglobulin heavy chain variable (IGHV) genes between plasmablasts clonally related to spike  
 717 binding mAbs from SARS-CoV-2 vaccinees, plasmablasts sorted from PBMCs one week after seasonal  
 718 influenza vaccination and found in vaccine-responding B cell clones, and naïve B cells found in blood of  
 719 an influenza vaccinee (left panel); and between plasmablasts from SARS-CoV-2 vaccinees found to be  
 720 clonally related to spike-binding mAbs that were, respectively, cross-reactive and non-cross-reactive to  
 721 human  $\beta$ -coronaviruses spike proteins (right panel). P values were generated using a two-sided Kruskal-  
 722 Wallis test with Dunn's post-test (left) or a Mann-Whitney U test (right).

723

724 **Figure 4. Mapping of the amino-acid substitutions and deletions onto the structure of the SARS-CoV-2**  
 725 **spike glycoprotein. A** lists mutations of the three major variants of concern B.1.17, B.1.315 and P.1. **B**  
 726 shows these mutations mapped onto the structure of the spike glycoprotein (model generated by  
 727 superposition of PDB 6M0j and 7C2L (Chi *et al.*, 2020; Lan *et al.*, 2020)). One RBD in the up conformation  
 728 (red) is bound with ACE2 receptor (pink). The NTD is colored blue and the various amino-acid  
 729 substitutions are shown as yellow spheres. One spike protomer is shown in bold colors while the other  
 730 two are colored white. **C** shows competition between ACE2 and neutralizing RBD targeting mAbs PVI.V3-  
 731 9 and PVI.V6-4 for binding to RBD. **D** BLI- measured binding affinities of the RBD mutants to ACE2, as  
 732 well as the calculated fold change, are shown in the table on the right.

733

734 **Figure 5. Binding and neutralization of SARS-CoV-2 variants.** Binding of serum samples from  
 735 convalescent individuals, vaccinees and vaccine derived mAbs to a panel of RBD mutants is shown in **A**,  
 736 **B and C** respectively. The red line in A indicates the average reduction. Dotted lines in A and B indicate  
 737 100%, the line with smaller dots in C indicated reactivity of the anti-his coating control. For vaccinees  
 738 late samples (V1=d89, V2=d102, V3=d47, V4=d48, V5=49 and V6=48) were assayed. **D** shows the spike  
 739 mutations of virus isolate PVI14252 modelled on a co-crystal structure of the SARS-CoV-2 spike protein  
 740 with ACE2 (model generated by superposition of PDB 6M0j and 7C2L (Chi *et al.*, 2020; Lan *et al.*, 2020)).  
 741 **E and F** show the inhibitory effect of vaccine serum and vaccine derived neutralizing antibodies on both  
 742 wild type SARS-CoV-2 and PV14252. **G** shows neutralizing activity of the plasmablast derived neutralizing  
 743 antibodies against wild type, B.1.1.7 and B.1.351 virus isolates. Of note, these comparative assays were  
 744 always performed side by side but sets are run by different operators and on a different Vero cell clone  
 745 as the neutralization assays shown in Figure 2.

746

747 **STAR Methods**748 **KEY RESOURCE TABLE**

749

| REAGENT or RESOURCE                                  | SOURCE                         | IDENTIFIER              |
|--|--------------------------------|-------------------------|
| <b>Antibodies</b>                                    |                                |                         |
| CD20-PB (clone 2H7)                                  | BioLegend                      | Cat#302320              |
| CD71-FITC (clone CY1G4)                              | BioLegend                      | Cat#334104              |
| IgD-PerCP-Cy5.5 (clone IA6-2)                        | BioLegend                      | Cat#348208              |
| CD19-PE (clone HIB19)                                | BioLegend                      | Cat#302254              |
| CD38-PE-Cy7 (clone HIT2)                             | BioLegend                      | Cat#303516              |
| CD3-Alexa 700 (clone HIT3a)                          | BioLegend                      | Cat#300324              |
| Streptavidin (HRP)                                   | Abcam                          | Cat#7403                |
| Biotin Anti-6X His tag® antibody                     | Abcam                          | Cat#27025               |
| Anti-mouse IgG HRP                                   | Rockland antibodies and assays | catalog #610-4302       |
| Mouse anti-histidine antibody                        | Takara                         | catalog #631212         |
| Anti-human IgG HRP                                   | Millipore Sigma                | catalog #A0293          |
| <b>Bacterial and virus strains</b>                   |                                |                         |
| SARS-CoV-2 (isolate USA - WA1/2020)                  | BEI                            | NR-52281                |
| SARS-CoV-2 patient isolate                           | PVI, Mount Sinai               | PV14252                 |
| SARS-CoV-2 hCoV-19/South Africa/KRISP-K005325/2020   | BEI                            | NR-54009                |
| SARS-CoV-2 Isolate hCoV-19/England/204820464/2020    | BEI                            | NR-54000                |
| <b>Biological samples</b>                            |                                |                         |
| Serum samples  | PVI, Mount Sinai               | V1-V6, 30 convalescents |
| Blood samples  | PVI, Mount Sinai               | V3, V5, V6              |
| <b>Chemicals, peptides, and recombinant proteins</b> |                                |                         |
| Zombie Aqua  | BioLegend                      | Cat#423101              |
| 10x Lysis Buffer                                     | Clontech                       | Cat#635013              |
| RNase Inhibitor, Murine                              | New England BioLabs            | Cat# M0314L             |
| Maxima H Reverse Transcriptase                       | Thermo                         | Cat#EP0753              |
| Protein A agarose                                    | Thermo                         | Cat#15918014            |
| Chromium Next GEM Single Cell 5' Kit v2              | 10X Genomics                   | Cat#1000263             |
| Library Construction Kit                             | 10X Genomics                   | Cat#1000190             |
| Chromium Next GEM Chip K Single Cell Kit             | 10X Genomics                   | Cat#1000286             |
| Chromium Single Cell Human BCR Amplification Kit     | 10X Genomics                   | Cat# 1000253            |
| Dual Index Kit TT Set A                              | 10X Genomics                   | Cat#1000215             |
| SPRIselect Reagent Kit                               | Beckman Coulter                | Cat# B23318             |
| High Sensitivity D5000 ScreenTape                    | Agilent                        | Cat# 5067-5592          |
| High Sensitivity D5000 Reagents                      | Agilent                        | Cat# 5067-5593          |

|  |                          |                 |
|--|--------------------------|-----------------|
| Bovine Serum Albumin   | Fisher Bioreagents       | Cat# BP9700-100 |
| SARS-CoV-2 RBD   | Krammer lab, Mount Sinai | N/A             |
| SARs-CoV-2 variant RBDs: E406Q, N417V, N439K, N440K, Y453F, E484K, F486A, N487R, F490K, Q493R, B.1.1.7, N439K/Y453F, B.1.351 and P.1 | Krammer lab, Mount Sinai | N/A             |
| SARS-CoV-2 Spike (2P)  | Krammer lab, Mount Sinai | N/A             |
| OC43 spike   | Krammer lab, Mount Sinai | N/A             |
| HKU spike  | Krammer lab, Mount Sinai | N/A             |
| 229E spike   | Krammer lab, Mount Sinai | N/A             |
| NL63 spike   | Krammer lab, Mount Sinai | N/A             |
| SARS-CoV-2 NTD   | Sino Biological          | 40591-V49H      |
| SARS-CoV-2 S2  | Sino Biological          | 40590-V02H      |
| Remdesivir   | NIH                      | N/A             |
| Critical commercial assays   |                          |                 |
| Anti-human IgG Fc Biosensors   | Sartorius Corporation    | Cat# 18-5001    |
| Ni-NTA (NTA) Biosensors  | Sartorius Corporation    | Cat# 18-5101    |
|  |                          |                 |
|  |                          |                 |
| Deposited data   |                          |                 |
| Human B cell receptor repertoire data after seasonal influenza vaccination   | Turner et al., 2020      | PRJNA610059     |
|  |                          |                 |
|  |                          |                 |
|  |                          |                 |
| Experimental models: cell lines  |                          |                 |
| Expi293F   | Gibco                    | Cat#A14527      |
| Vero.E6 cells  | ATCC                     | #CRL - 1586     |
| Expi293F   | Thermo Fisher            | A14528          |
|  |                          |                 |
|  |                          |                 |
| Experimental models: organisms/strains   |                          |                 |
|  |                          |                 |
|  |                          |                 |
|  |                          |                 |
|  |                          |                 |
|  |                          |                 |
| Oligonucleotides   |                          |                 |
| oligo-dT <sub>23</sub> VN primer, random Hexamers  | Integrated DNA           | N/A             |

|   |   |   |
|---|---|---|
|   | Technologies  |   |
| 1 <sup>st</sup> PCR primers & nested PCR primers  | Smith et al., 2009  | N/A   |
| Gibson Cloning Primers  | Ho et al., 2009   | N/A   |
| M13 Reverse (-27)   | Integrated DNA Technologies   | 51-01-13-03   |
|   |   |   |
|   |   |   |
| <b>Recombinant DNA</b>  |   |   |
| pCAGGS  | <a href="https://www.ncbi.nlm.nih.gov/pmc/articles/PMC4248980/">https://www.ncbi.nlm.nih.gov/pmc/articles/PMC4248980/</a> | N/A   |
| pCAGGS SARS-CoV-2   | <a href="https://pubmed.ncbi.nlm.nih.gov/32398876/">https://pubmed.ncbi.nlm.nih.gov/32398876/</a>                         | N/A   |
| pCAGGS SARS-CoV-2 SA variant spike  | This paper  | N/A   |
| pCAGGS SARS-CoV-2 UK variant spike  | This paper  | N/A   |
| pCAGGS SARS-CoV-2 RBD   | <a href="https://pubmed.ncbi.nlm.nih.gov/32398876/">https://pubmed.ncbi.nlm.nih.gov/32398876/</a>                         | N/A   |
| pCAGGS SARS-CoV-2 variant RBDs: E406Q, N417V, N439K, N440K, Y453F, E484K, F486A, N487R, F490K, Q493R, B.1.1.7, N439K/Y453F, B.1.351 and P.1 | This paper  | N/A   |
| OC43 2P spike plasmid   | <a href="https://www.ncbi.nlm.nih.gov/pmc/articles/PMC5584442/">https://www.ncbi.nlm.nih.gov/pmc/articles/PMC5584442/</a> | N/A   |
| HKU1 2P spike plasmid   | <a href="https://www.ncbi.nlm.nih.gov/pmc/articles/PMC5584442/">https://www.ncbi.nlm.nih.gov/pmc/articles/PMC5584442/</a> | N/A   |
| <b>Software and algorithms</b>  |   |   |
| Cell Ranger (v5)  | 10x Genomics  | <a href="https://www.support.10xgenomics.com">https://www.support.10xgenomics.com</a>   |
| Seurat (v3.2.2)   | Stuart & Butler, et al 2019   | <a href="https://satijalab.org/seurat/">https://satijalab.org/seurat/</a>   |
| scRepertoire (v1.1.3)   | Borcherding, et al, 2020  | <a href="https://github.com/ncborcherding/scRepertoire">https://github.com/ncborcherding/scRepertoire</a>   |
| schex (v1.3.0)  | Saskia Freytag  | <a href="https://github.com/SaskiaFreytag/schex">https://github.com/SaskiaFreytag/schex</a>   |
| IgBLAST v1.14.0   | Ye et al., 2013   | <a href="https://ftp.ncbi.nih.gov/blast/executables/igblast/release/1.14.0/">https://ftp.ncbi.nih.gov/blast/executables/igblast/release/1.14.0/</a> |
| Change-O v0.4.6   | Gupta et al., 2015  | <a href="http://changeo.readthedocs.io/">http://changeo.readthedocs.io/</a>   |
| SHazaM v1.0.2   | Gupta et al., 2015  | <a href="http://shazam.readthedocs.io/">http://shazam.readthedocs.io/</a>   |
| GraphPad Prism v9.0.2   | GraphPad Software   | <a href="http://www.graphpad.com">www.graphpad.com</a>  |
| BLItz Pro 1.3.1.3   | Forté Bio   | <a href="http://www.fortebio.com/blitz.html">www.fortebio.com/blitz.html</a>  |

|   |                         |   |
|---|-------------------------|---|
| Microsoft Excel   | Microsoft               | <a href="https://www.microsoft.com/en-ww/microsoft-365/excel">https://www.microsoft.com/en-ww/microsoft-365/excel</a> |
| Other   |                         |   |
| International ImMunoGeneTics Information System (IMGT) human immunoglobulin germline references, release 201931-4 | Giudicelli et al., 2005 | <a href="http://www.imgt.org/vquest/refseqh.html#refdir">http://www.imgt.org/vquest/refseqh.html#refdir</a>           |
|   |                         |   |
|   |                         |   |
|   |                         |   |

750

751 **RESOURCE AVAILABILITY**752 **Lead contact**

753 Requests for information or reagents should be directed to Florian Krammer  
754 (florian.krammer@mssm.edu).

755 **Materials availability**

756 Plasmids for SARS-CoV-2 antigens have been deposited at BEI Resources and can also be requested from  
757 the authors. Plasmids for human coronavirus spikes can be requested from NIH's Vaccine Research  
758 Center. MAbs and plasmids for mAb expression can be obtained from the authors upon reasonable  
759 request. Variant viruses can be sourced from BEI Resources.

760 **Data and code availability**

761 The published article contains all data sets analyzed during the study except for BCR sequencing data  
762 which can be requested from Ali H. Ellebedy upon reasonable request.

763 **EXPERIMENTAL MODEL AND SUBJECT DETAILS**

764 **Human subjects and specimen collection.** The study protocols for the collection of clinical specimens  
765 from individuals with and without SARS-CoV-2 infection by the Personalized Virology Initiative were  
766 reviewed and approved by the Mount Sinai Hospital Institutional Review Board (IRB-16-16772; IRB-16-  
767 00791; IRB-20-03374). All participants provided written informed consent prior to collection of specimen  
768 and clinical information. All specimens were coded prior to processing and analysis. An overview of the  
769 characteristics of the vaccinees as well as the study participants with and without COVID-19 is provided  
770 in **Suppl. Table 1**. The vaccinees received two doses of the Pfizer mRNA vaccine.

771 Whole blood was collected via phlebotomy in serum separator tubes (SST) or  
772 ethylenediaminetetraacetic acid (EDTA) tubes. Serum was collected after centrifugation as per  
773 manufacturers' instructions. Peripheral blood mononuclear cells (PBMCs) isolation was performed by  
774 density gradient centrifugation using SepMate tubes (Stemcell) according to manufacturers'  
775 instructions. PBMCs were cryo-preserved and stored in liquid nitrogen until analysis.

776 **Recombinant proteins.** All recombinant proteins were produced using Expi293F cells (Life  
777 Technologies). Receptor binding domain (RBD) and spike protein of SARS-CoV-2 (GenBank:  
778 MN908947.3) was cloned into a mammalian expression vector, pCAGGS as described earlier (Amanat et  
779 al., 2020b; Stadlbauer et al., 2020). RBD mutants were generated in the pCAGGS RBD construct by  
780 changing single residues using mutagenesis primers. All proteins were purified after transient  
781 transfections with each respective plasmid. Six-hundred million Expi293F cells were transfected using  
782 the ExpiFectamine 293 Transfection Kit and purified DNA. Supernatants were collected on day four post  
783 transfection, centrifuged at 4,000 g for 20 minutes and finally, the supernatant was filtered using a 0.22  
784  $\mu\text{m}$  filter. Ni-NTA agarose (Qiagen) was used to purify the protein via gravity flow and proteins were  
785 eluted as previously described (Amanat *et al.*, 2020b; Stadlbauer *et al.*, 2020). The buffer was exchanged  
786 using Amicon centrifugal units (EMD Millipore) and all recombinant proteins were finally re-suspended  
787 in phosphate buffered saline (PBS). Proteins were also run on a sodium dodecyl sulphate (SDS)  
788 polyacrylamide gels (5–20% gradient; Bio-Rad) to check for purity (Amanat et al., 2018; Margine et al.,  
789 2013). Plasmids to express recombinant spike proteins of 229E, HKU1, NL63 and OC43 were generously  
790 provided by Dr. Barney Graham (Pallesen et al., 2017). NTD and S2 proteins were purchased from  
791 SinoBiologics.

## 792 **METHOD DETAILS**

793  
794 **ELISA.** Ninety-six well plates (Immulon 4 HBX; Thermo Scientific) were coated overnight at 4°C with  
795 recombinant proteins at a concentration of 2  $\mu\text{g}/\text{ml}$  in PBS (Gibco; Life Technologies) and 50  $\mu\text{l}$ /well.  
796 The next day, the coating solution was discarded. One hundred  $\mu\text{l}$  per well of 3% non-fat milk prepared  
797 in PBS (Life Technologies) containing 0.01% Tween-20 (TPBS; Fisher Scientific) was added to the plates to  
798 block the plates for 1 hour at room temperature (RT). All serum dilutions were prepared in 1% non-fat  
799 milk prepared in TPBS. All serum samples were diluted 3-fold starting at a dilution of 1:50. After the  
800 blocking step, serum dilutions were added to the respective plates for two hours at RT. Next, plates  
801 were washed thrice with 250  $\mu\text{l}$ /well of TPBS to remove any residual primary antibody. Secondary  
802 antibody solution was prepared in 1% non-fat milk in TPBS as well and 100  $\mu\text{l}$ /well was added to the  
803 plates for 1 hour at RT. For human samples, anti-human IgG conjugated to horseradish peroxidase (HRP)  
804 was used at a dilution of 1:3000 (Millipore Sigma; catalog #A0293). For mouse samples, anti-mouse IgG  
805 conjugated to HRP was used at the same dilution (Rockland antibodies and assays; catalog #610-4302).  
806 Specifically, a mouse anti-histidine antibody (Takara; catalog #631212) was used as a positive control to  
807 detect proteins with a hexa-histidine tag. Once the secondary incubation was done, plates were again  
808 washed thrice with 250  $\mu\text{l}$ /well of TPBS. Developing solution was made in 0.05M phosphate-citrate  
809 buffer at pH 5 using o-phenylenediamine dihydrochloride tablets (Sigma-Aldrich; OPD) at a final  
810 concentration of 0.04  $\text{mg}/\text{ml}$ . One hundred  $\mu\text{l}$ /well of developing solution was added to each plate for  
811 exactly 10 minutes after which the reaction was halted with addition of 50  $\mu\text{l}$ /well of 3M hydrochloric  
812 acid (HCl). Plates were read at an optical density of 490 nanometers using a Synergy 4 (BioTek) plate  
813 reader. Eight wells on each plate received no primary antibody (blank wells) and the optical density in  
814 those wells was used to assess background. Area under the curve was calculated by deducting the  
815 average of blank values plus 3 times standard deviation of the blank values. All data was analyzed in  
816 Graphpad Prism 7. This protocol has been described in detail earlier (Bailey et al., 2019; Wohlbold et al.,  
817 2015).

818 Purified monoclonal antibodies were used at a concentration of 30 ug/ml and then subsequently diluted  
819 3-fold. Purified monoclonal antibodies were only incubated on the coated plates for an hour. The  
820 remaining part of the protocol was the same as above (Amanat et al., 2020a; Wohlbold et al., 2016).

821 **Bio-layer Interferometry Binding Experiments.** Bio-layer Interferometry (BLI) experiments were  
822 performed using the BLItz system (fortéBIO, Pall Corporation). Recombinant human Fc fusion ACE2  
823 (SinoBiological) was immobilized on an anti-human IgG Fc biosensor, and RBDs were then applied to  
824 obtain binding affinities. Single-hit concentrations were tested at 5.8  $\mu$ M for binding. All measurements  
825 were repeated in subsequent independent experiments.  $K_D$  values were obtained through local fit of the  
826 curves by applying a 1:1 binding isotherm model using vendor-supplied software. All experiments were  
827 performed in PBS pH 7.4 and at room temperature.

828  
829 **hACE2 competition interferometry experiments,** Interferometry experiments were performed using a  
830 BLItz instrument (fortéBIO, Sartorius). Polyhistidine-tagged Fabs were immobilized on Ni-NTA biosensors  
831 at 10  $\mu$ g/ml and SARS-CoV-2 RBD was supplied as analyte at 5 $\mu$ M alone or pre-mixed with hACE2-Fc at  
832 different concentrations. Maximal signal at association ( $R_{max}$ ) was used to plot the concentration-  
833 dependent competition with hACE2. All experiments were performed in PBS at pH 7.4 and at room  
834 temperature.

835  
836 **RBD-hACE2 ELISA.** 25ng of hACE2-Fc fusion protein expressed in HEK293 cells were adhered to high-  
837 capacity binding, 96 well-plates (Corning) overnight in PBS. Plates were blocked with 5% BSA in PBS  
838 containing Tween-20 (PBS-T) for 1hr at room temperature (RT). Blocking solution was discarded and 5-  
839 fold dilutions of 6xHis-tagged RBDs in PBS were added to wells and incubated for 1hr at RT. Plates were  
840 then washed three times with PBS-T. Anti-polyhistidine IgG-Biotin (Abcam) in PBS-T was added to each  
841 and incubated for 1hr at RT. Plates were then washed three times with PBS-T. Streptavidin-HRP (Abcam)  
842 in PBS-T was added to each and incubated for 1hr at RT. Plates were then washed three times with PBS-  
843 T Plates were developed using 1-Step Ultra TMB substrate (ThermoFisher), stopped with sulfuric acid  
844 and immediately read using a plate reader at 450nm. Data were plotted using Prism 9 (GraphPad  
845 Software) and affinities determined by applying a nonlinear regression model.

846  
847 **Viruses and cells.** Vero.E6 cells (ATCC #CRL-1586) cells were maintained in culture using Dulbecco's  
848 Modified Eagles Medium (DMEM, Gibco) which was supplemented with 10% fetal bovine serum (FBS,  
849 Corning) and antibiotics solution containing 10,000 units/mL of penicillin and 10,000  $\mu$ g/mL of  
850 streptomycin (Pen Strep, Gibco)(10). Wild type SARS-CoV-2 (isolate USA-WA1/2020), hCoV-19/South  
851 Africa/KRISP-K005325/2020 (B.1.351, BEI Resources NR-54009) and hCoV-19/England/204820464/2020  
852 (B.1.1.7, BEI Resources NR-54000) were grown in cells for 3 days, the supernatant was clarified by  
853 centrifugation at 4,000 g for 5 minutes and aliquots were frozen at -80°C for long term use. The viruses  
854 were subjected to deep sequencing to ensure that no mutations had taken place in culture. The  
855 polybasic cleavage site changed to WRAR in the B.1.351 variant virus during cultivation in cell culture (as  
856 known for this virus at BEI Resources) and no other unexpected mutations occurred. A primary virus  
857 isolate, PV14252, bearing mutations and deletions in the spike was obtained by incubating 200 uls of  
858 viral transport media from the nasopharyngeal swab with Vero.E6 cells. The sequence of the passage 2  
859 viral isolate was identical to the sequence obtained directly from the clinical specimen. Sequencing was  
860 performed on the Illumina platform as described previously (Gonzalez-Reiche et al., 2020). Both  
861 replication competent viruses were used to test serum from study participants and antibodies for  
862 neutralization activity.

863

864 **Neutralization assay.** Twenty-thousand cells in 100  $\mu$ l per well were seeded on sterile 96-well cell  
865 culture plates one day prior to the neutralization assay. In general, cells were used at 90% confluency to  
866 perform the assay. All serum samples were heat-inactivated to eliminate any complement activity. Serial  
867 dilutions of serum samples were made in 1X minimal essential medium (MEM; Life Technologies)  
868 starting at a dilution of 1:20. All work with authentic SARS-CoV-2 (isolate USA-WA1/2020 and PV14252)  
869 was done in a biosafety level 3 (BSL3) laboratory following institutional biosafety guidelines and has  
870 been described in much greater detail earlier (Amanat *et al.*, 2020b; Amanat *et al.*, 2020c). Six hundred  
871 median cell culture infectious doses (TCID<sub>50</sub>s) of authentic virus (USA-WA1/2020 and PV14252) was  
872 added to each serum dilution and virus-serum mixture was incubated together for 1 hour inside the  
873 biosafety cabinet. Media from the cells was removed and 120  $\mu$ l of the virus-serum mixture was added  
874 onto the cells for 1 hour at 37°C. After one hour, the virus-serum mixture was removed and 100  $\mu$ l of  
875 each corresponding dilution was added to every well. In addition, 100  $\mu$ l of 1X MEM was also added to  
876 every well. Cells were incubated for 48 hours at 37°C after which the media was removed and 150  $\mu$ l of  
877 10% formaldehyde (Polysciences) was added to inactivate the virus. For assay control, remdesivir was  
878 used against both the wild type virus as well as the patient isolate. After 24 hours, cells were  
879 permeabilized and stained using an anti-nucleoprotein antibody 1C7 as discussed in detail earlier  
880 (Amanat *et al.*, 2020b; Sun *et al.*, 2020).

881 **Cell sorting and flow cytometry.** Staining for sorting was performed using cryo-preserved PBMCs in 2%  
882 FBS and 2 mM ethylenediaminetetraacetic acid (EDTA) in PBS (P2). Cells were stained for 30 min on ice  
883 with CD20-Pacific Blue (2H7, 1:400), Zombie Aqua, CD71-FITC (CY1G4, 1:200), IgD-PerCP-Cy5.5 (IA6-2,  
884 1:200), CD19-PE (HIB19, 1:200), CD38-PE-Cy7 (HIT2, 1:200), and CD3-Alexa 700 (HIT3a, 1:200), all  
885 BioLegend. Cells were washed twice, and single plasmablasts (live singlet CD19<sup>+</sup> CD3<sup>-</sup> IgD<sup>lo</sup> CD38<sup>+</sup> CD20<sup>-</sup>  
886 CD71<sup>+</sup>) were sorted using a FACSAria II into 96-well plates containing 2  $\mu$ l Lysis Buffer (Clontech)  
887 supplemented with 1 U/ $\mu$ l RNase inhibitor (NEB) and immediately frozen on dry ice, or bulk sorted into  
888 PBS supplemented with 0.05% BSA and processed for single cell RNAseq.

889 **Monoclonal antibody (mAb) generation.** Antibodies were cloned as described previously (Wrarmert *et al.*,  
890 2011). Briefly, VH, V $\kappa$ , and V $\lambda$  genes were amplified by reverse transcription-PCR and nested PCR  
891 reactions from singly sorted plasmablasts using primer combinations specific for IgG, IgM/A, Ig $\kappa$ , and Ig $\lambda$   
892 from previously described primer sets (Smith *et al.*, 2009) and then sequenced. To generate  
893 recombinant antibodies, restriction sites were incorporated via PCR with primers to the corresponding  
894 heavy and light chain V and J genes. The amplified VH, V $\kappa$ , and V $\lambda$  genes were cloned into IgG1 and Ig $\kappa$   
895 expression vectors, respectively, as described previously (Nachbagauer *et al.*, 2018; Wrarmert *et al.*,  
896 2008). Heavy and light chain plasmids were co-transfected into Expi293F cells (Gibco) for expression,  
897 and antibody was purified with protein A agarose (Invitrogen).

898 **Single-cell RNAseq library preparation and sequencing.** Bulk-sorted plasmablasts were processed using  
899 the following 10 $\times$  Genomics kits: Chromium Next GEM Single Cell 5' Kit v2 (PN-1000263); Library  
900 Construction Kit (PN-1000190); Chromium Next GEM Chip K Single Cell Kit (PN-1000286); Chromium  
901 Single Cell Human BCR Amplification Kit (PN-1000253), and Dual Index Kit TT Set A (PN-1000215). The  
902 cDNAs were prepared after GEM generation and barcoding, followed by GEM RT reaction and bead  
903 cleanup steps. Purified cDNA was amplified for 10–14 cycles before cleaning with SPRIselect beads.  
904 Then, samples were evaluated on a 4200 TapeStation (Agilent) to determine cDNA concentration. B-cell  
905 receptor (BCR) target enrichments were performed on full-length cDNA. Gene expression and enriched  
906 BCR libraries were prepared as recommended by the Chromium Next GEM Single Cell 5' Reagent Kits v2  
907 (Dual Index) user guide, with appropriate modifications to the PCR cycles based on the calculated cDNA  
908 concentration. The cDNA libraries were sequenced on Novaseq S4 (Illumina), targeting a median

909 sequencing depth of 50,000 and 5,000 read pairs per cell for gene expression and BCR libraries,  
910 respectively.

911 **Single cell RNAseq analysis.** Single-cell RNA sequencing and BCR sequencing data was processed using  
912 Cell Ranger v5.0 and the GRCh38-2020 version of the human genome provided by the manufacturer.  
913 Total recovered cells by RNA sequencing were V3: 6,608, V5: 5,256, and V6: 6,325 with a mean of  
914 90.64% read mapped to the genome. Count matrices were processed in R (v4.0.2) using the Seurat  
915 (v3.2.2) R package (Stuart et al., 2019). Cells were filtered for percentage of mitochondrial genes less  
916 than 15% and number features less than 4,000. The three specimen sequencing runs were integrated  
917 using log-normalized count values and canonical correlation approach (Stuart *et al.*, 2019) with 2,000  
918 variable features. The resulting single-cell object underwent principal component analysis and the top  
919 30 principal components were used for uniform manifold approximation and projection and identifying  
920 neighbors. Clustering was performed using a resolution of 0.6. The integrated RNA sequencing object  
921 included 12,568 cells with V3: 4,584, V5: 3,523, and V6: 4,461 cells. The filtered contig annotation  
922 output of Cell Ranger vdj were loaded into R and processed using the scRepertoire (v1.1.3) R package  
923 (Borcherding et al., 2020). Clonotypes were assigned using igraph (v1.2.6) network analysis of  
924 components generated from CDR3 sequences greater than or equal to 0.85 normalized Levenshtein  
925 distance. Percent of cells expressing genes along the UMAP embedding was visualized using the schex  
926 (v1.3.0) R package. For mutation analysis, heavy chains of mAbs and single-cell BCRs first underwent  
927 V(D)J gene annotation using IgBLAST (v1.14.0) (Ye et al., 2013) with human reference (release 201931-4)  
928 from the international ImMunoGeneTics information system (IMGT) (Giudicelli et al., 2005) and then  
929 parsing using Change-O (v0.4.6) (Gupta et al., 2015). Mutation frequency was calculated, as described in  
930 (Turner *et al.*, 2020), using the "calcObservedMutations" function from SHazaM (v.1.0.2) (Gupta *et al.*,  
931 2015) and by counting the number of nucleotide mismatches from the germline sequence in the heavy  
932 chain variable segment leading up to the complementary-determining region 3 (CDR3), while excluding  
933 the first 18 positions that could be error-prone due to the primers used for generating the mAb  
934 sequences.

935

## 936 **QUANTIFICATION AND STATISTICAL ANALYSIS**

937 **Structure visualization and statistical analysis.** Structural figures were modeled and rendered in Pymol  
938 (The PyMOL Molecular Graphics System, Version 2.4 Schrödinger, LLC). Statistical analysis was  
939 performed in GraphPad Prism using a one-way ANOVA with correction for multiple comparisons for  
940 Supplementary Figure 1. For Figure 3, p values were generated using a two-sided Kruskal-Wallis test  
941 with Dunn's post-test or a Mann-Whitney U test. Significance was defined as  $p < 0.05$ , p values are  
942 directly indicated in graphs. Number of subjects can be found in the results and methods section,  
943 definition of center, and dispersion and precision measures are described in the respective figure  
944 legends.

945

## 946 **ADDITIONAL RESOURCES**

947 Not applicable.

948

## 949 **Supplementary Figure Legends**

950

951 **Supplementary Figure 1. Full length spike to RBD ratios (A) and comparison of binding to neutralizing**  
952 **titer ratios between naturally infected and vaccinated individuals (B) (related to Figure 1).** Statistical  
953 analysis was performed in GraphPad Prism using a one-way ANOVA with correction for multiple  
954 comparisons, significance was defined as  $p < 0.05$ .

955

956 **Supplementary Figure 2. Gating strategy for sorting plasmablasts from total PBMCs isolated one week**  
957 **after second immunization (related to Figure 2 and 3).**

958

959 **Supplementary Figure 3. Representative Biolayer Interferometry binding isotherms from two**  
960 **independent experiments. The raw data are show in pink and the Langmuir 1:1 kinetics fit is show in**  
961 **black (related to Figure 4).**

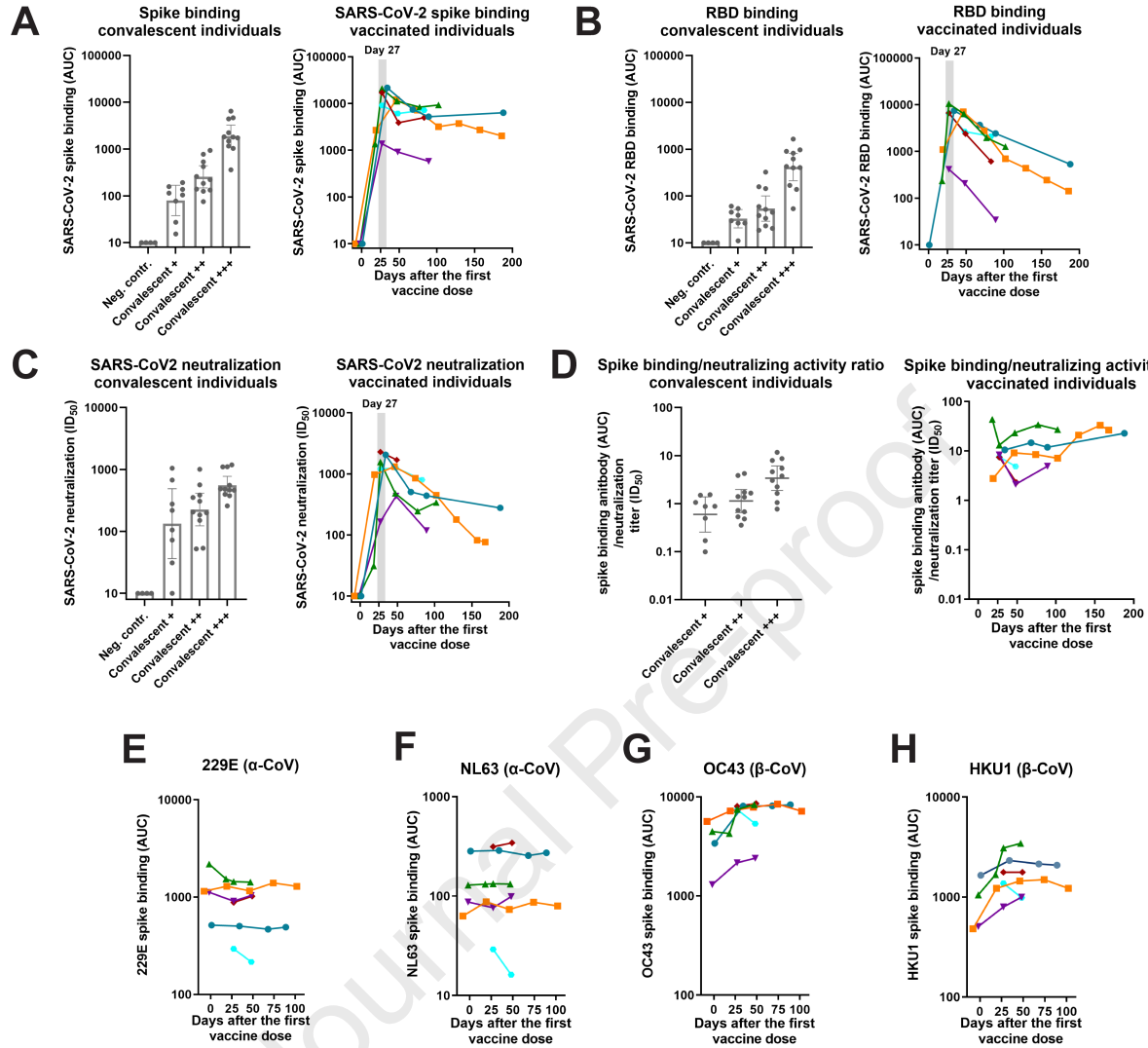
962

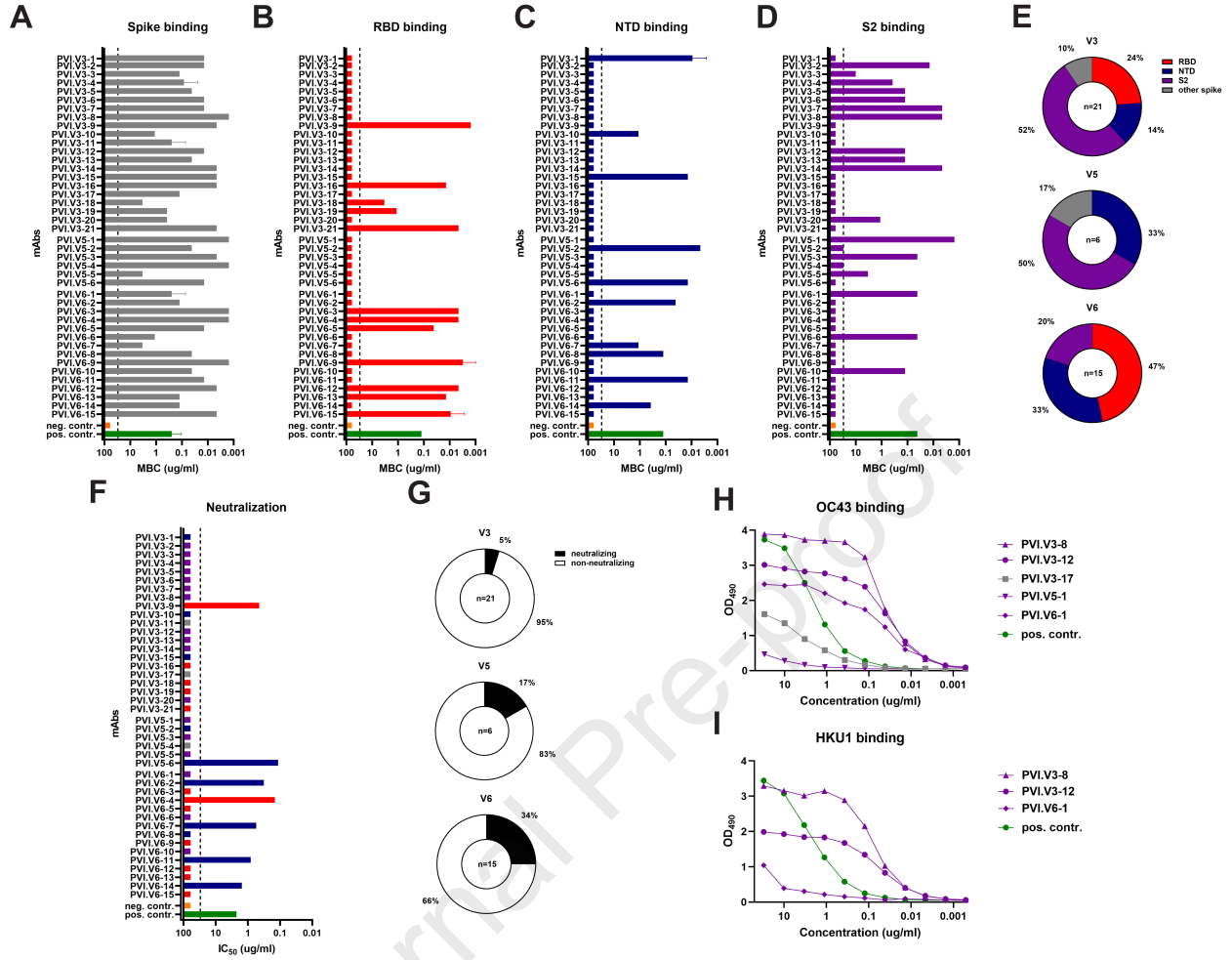
963 **Supplementary Figure 4. Binding of SARS-CoV-2 variant RBDs to ACE2. A** ELISA curves of the RBD  
964 variants binding to human ACE2. Shown are the binding curves calculated with nonlinear regression to  
965 the arithmetic mean values from eight replicates  $\pm$  SEM. The calculated steady-state  $K_D$  values  $\pm$  SEM  
966 from end-point ELISA measurements and the fold-change in comparison to wild type RBD are reported  
967 in **B** (related to Figure 4).

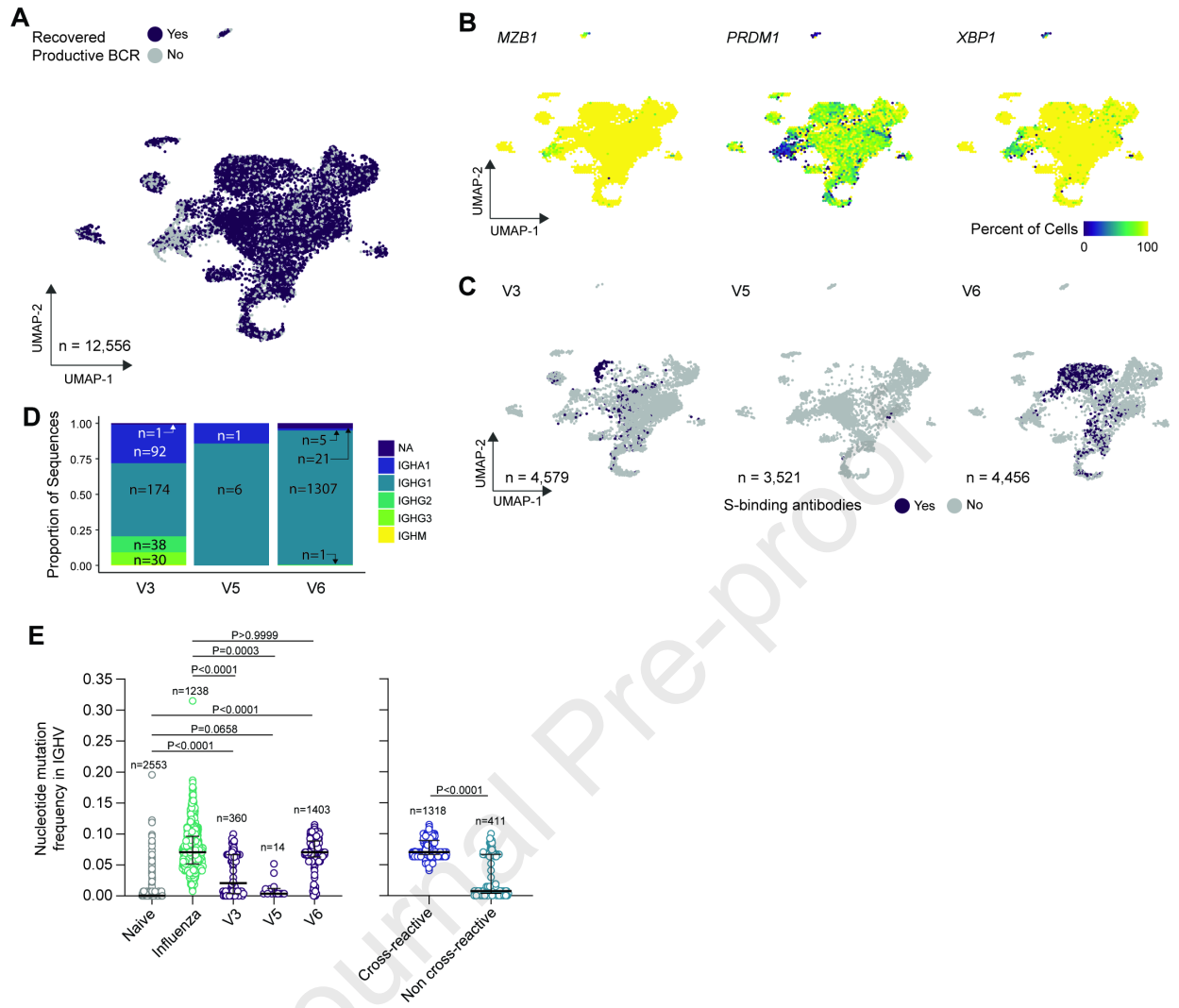
968

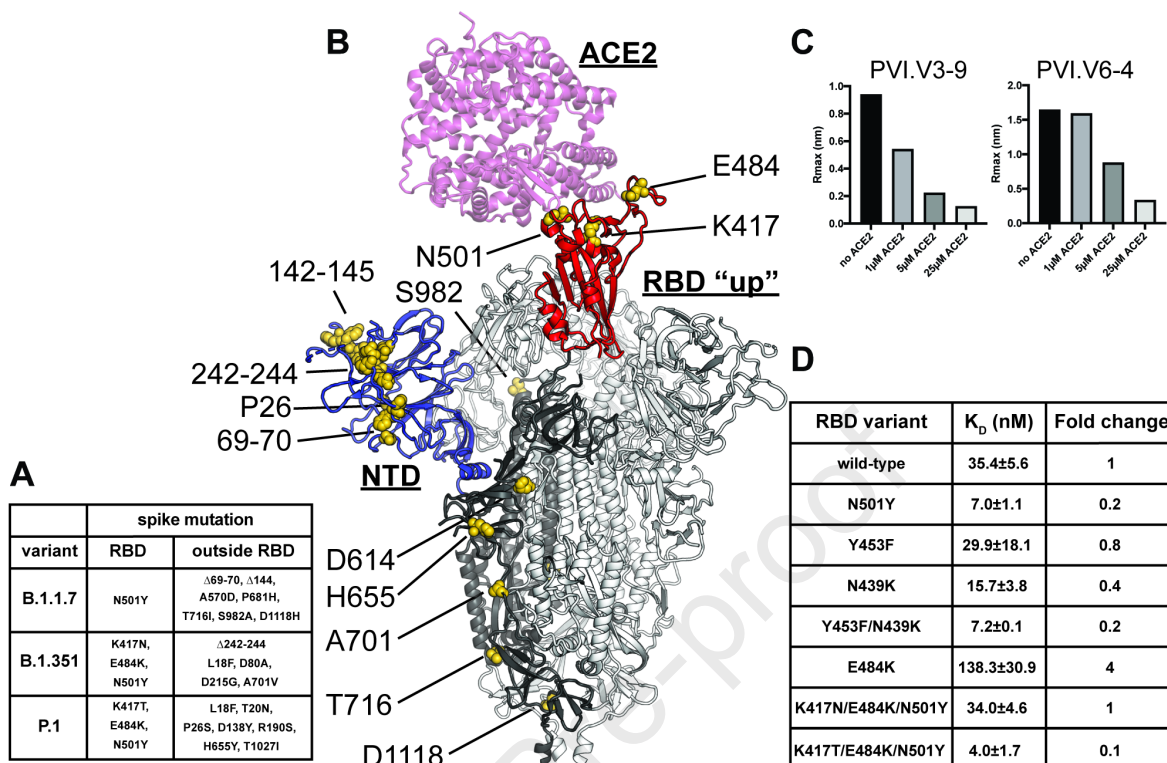
- Antibody responses after SARS-CoV-2 mRNA vaccination target RBD, NTD and S2
- SARS-CoV-2 mRNA vaccination induces a high rate of non-neutralizing antibodies
- Crossreactive antibodies to seasonal  $\beta$ -coronaviruses are induced by vaccination
- Variant mutation N501Y enhances affinity to human ACE2 while E484K reduces it

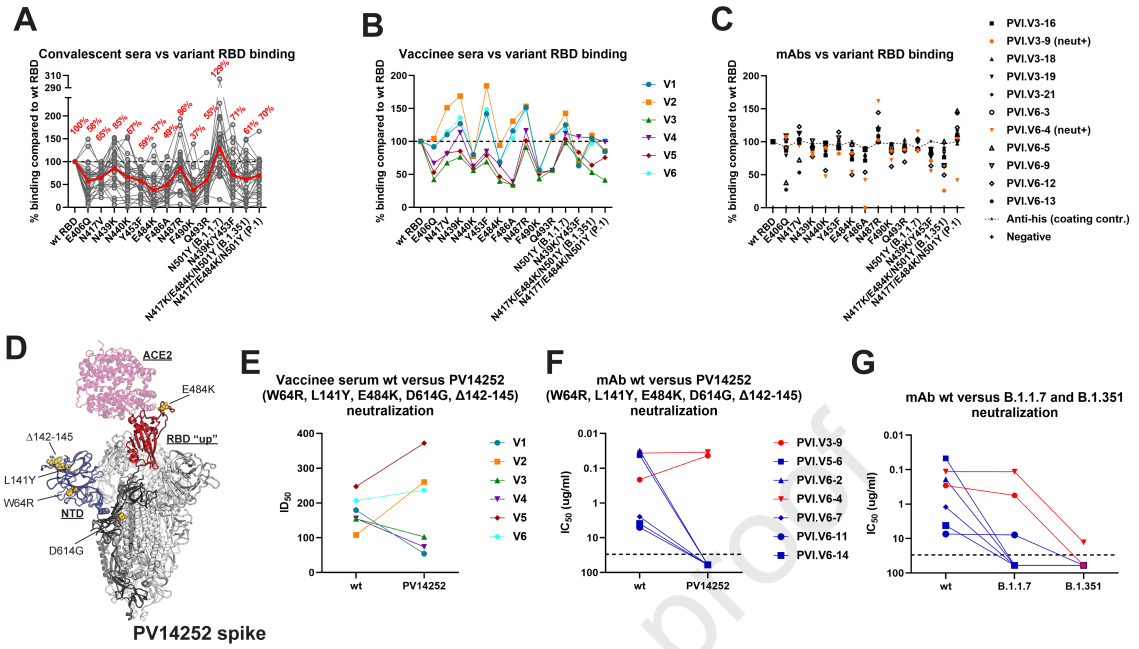
An analysis of mRNA vaccine-induced polyclonal antibodies and plasmablast derived monoclonal antibodies from individuals vaccinated against SARS-CoV-2 identifies a high proportion of non-neutralizing antibodies, the induction of cross-reactive antibodies to seasonal coronaviruses and also maps the regions in the spike protein that are targeted, even among viral variants.

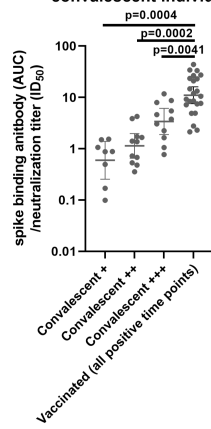
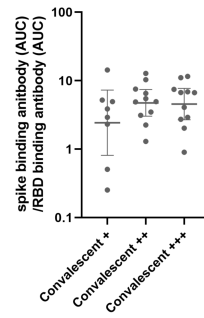
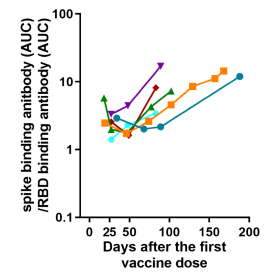


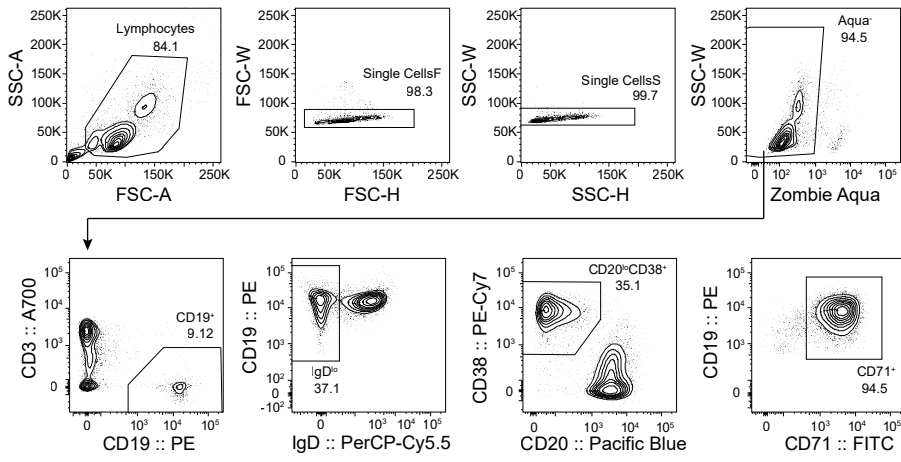




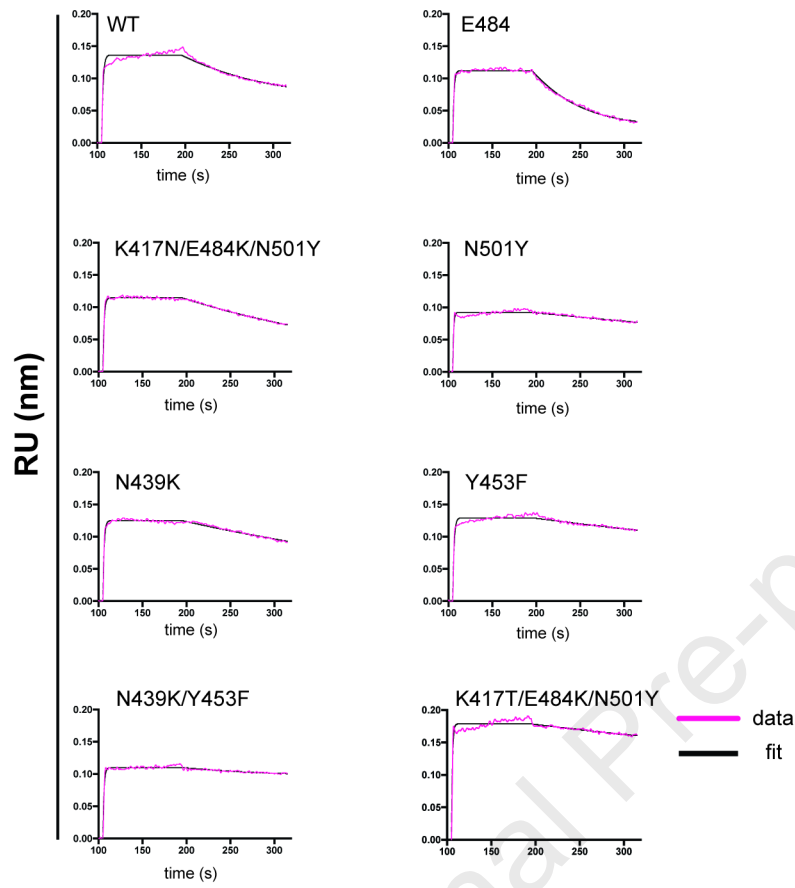


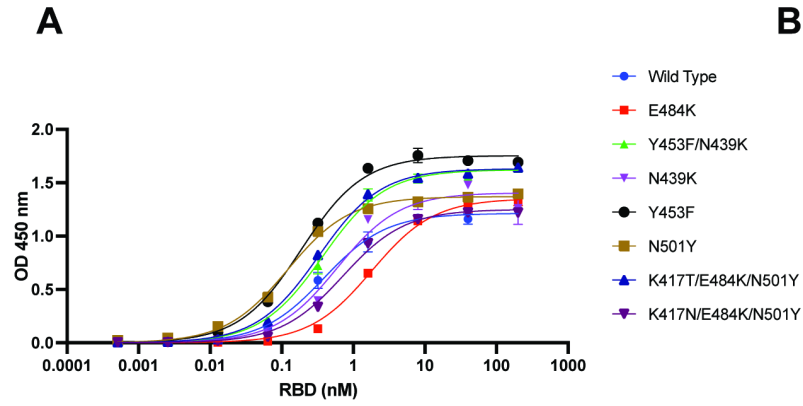


**A**Spike binding/neutralizing activity ratio  
convalescent individuals**B**Ratio spike binding/RBD binding antibodies  
convalescent individualsRatio spike binding/RBD binding antibodies  
vaccinated individuals



Journal Pre-proof





**B**

| RBD variant       | $K_D(10^{-11}M)$ | Fold change |
|-------------------|------------------|-------------|
| wild-type         | 38.8±0.5         | 1           |
| N501Y             | 12±0.1           | 0.3         |
| Y453F             | 18.9±0.1         | 0.5         |
| N439K             | 59.8±9.3         | 1.5         |
| Y453F/N439K       | 37.4±0.3         | 1           |
| E484K             | 181.9±14.5       | 4.7         |
| K417N/E484K/N501Y | 71.3±3.7         | 1.8         |
| K417T/E484K/N501Y | 32.9±1.3         | 0.8         |

Supplemental Table 1: Study participant and biospecimen information (related to Figure 1)

| Vaccinees                              | Spike IgG response <sup>1*</sup> | Sex        | Age group (yrs)        | Specimen tested  |
|--|----------------------------------|------------|------------------------|--|
| V1                                     | Strong positive                  | F          | >60                    | several longitudinal time points including days 34, 68, 89 and 188 post vaccination                |
| V2                                     | Strong positive                  | M          | 30-40                  | several longitudinal time points including days 19, 47, 74, 102, 129, 157 and 186 post vaccination |
| V3                                     | Strong positive                  | F          | 50-60                  | several longitudinal time points including days 19, 27, 47, 77 and 102 post vaccination            |
| V4                                     | Strong positive                  | M          | >60                    | several longitudinal time points including days 27, 48 and 89 post vaccination                     |
| V5                                     | Strong positive                  | F          | 40-50                  | several longitudinal time points including 27, 49 and 83 days post vaccination                     |
| V6                                     | Strong positive                  | F          | 30-40                  | several longitudinal time points including 27, 48 and 83 days post vaccination                     |
| <b>Seronegative, post pandemic</b>     |                                  | <b>Sex</b> | <b>Age group (yrs)</b> | <b>Days from last negative serology test when the sample was taken</b>                             |
| N1                                     | Negative                         | F          | 40-50                  | 23   |
| N2                                     | Negative                         | F          | 20-29                  | 24   |
| N3                                     | Negative                         | F          | 20-29                  | 23   |
| N4                                     | Negative                         | F          | 30-35                  | 22   |
| <b>Seropositive, natural infection</b> |                                  | <b>Sex</b> | <b>Age group (yrs)</b> | <b>Days post onset of COVID-19 symptoms when the sample was taken</b>                              |
| P1                                     | Weak positive                    | M          | 20-29                  | 260  |

|     |                   |   |       |                   |
|-----|-------------------|---|-------|-------------------|
| P2  | Weak positive     | M | 50-59 | no data available |
| P3  | Weak positive     | F | 30-39 | 111               |
| P4  | Weak positive     | F | 30-39 | 221               |
| P5  | Weak positive     | F | 30-39 | 254               |
| P6  | Weak positive     | F | 20-29 | 247               |
| P7  | Weak positive     | M | 30-39 | 220               |
| P8  | Weak positive     | F | 20-29 | Asymptomatic      |
| P9  | Moderate positive | M | 30-39 | no data available |
| P10 | Moderate positive | F | 30-39 | 197               |
| P11 | Moderate positive | F | 50-59 | Asymptomatic      |
| P12 | Moderate positive | F | 30-39 | Asymptomatic      |
| P13 | Moderate positive | M | 30-39 | 234               |
| P14 | Moderate positive | F | 20-29 | 273               |
| P15 | Moderate positive | M | 30-39 | Asymptomatic      |
| P16 | Moderate positive | F | 20-29 | 258               |
| P17 | Moderate positive | F | 20-29 | 246               |
| P18 | Moderate positive | M | 20-29 | Asymptomatic      |
| P19 | Moderate positive | F | 50-59 | 204               |
| P20 | Strong positive   | F | 50-59 | no data available |
| P21 | Strong positive   | F | 30-39 | 245               |
| P22 | Strong positive   | M | NA    | 170               |
| P23 | Strong positive   | F | >60   | Asymptomatic      |
| P24 | Strong positive   | F | 40-49 | no data available |
| P25 | Strong positive   | F | 50-59 | 191               |
| P26 | Strong positive   | F | 30-39 | no data available |
| P27 | Strong positive   | F | 50-59 | 113               |
| P28 | Strong positive   | M | >60   | Asymptomatic      |
| P29 | Strong positive   | M | 18-19 | 218               |
| P30 | Strong positive   | M | 50-59 | 219               |

<sup>1</sup>Samples were categorized based on initial titers obtained from Mount Sinai's CLIA laboratory test. Weak positive: 1:80 – 1:160 weak positive; 1:320-1:960 moderate positive; 1:960-1: ≥2880 strong positive

\* All six vaccinees were sero-negative for SARS-CoV-2 without clinical evidence of COVID19 prior to SARS-CoV-2 spike mRNA vaccination.

**Supplemental Table 2: Immunoglobulin gene usage of the spike-mAbs (related to Figure 2 and 3)**

| Name      | Native isotype | Heavy chain        |                           | Light chain |                   |
|-----------|----------------|--------------------|---------------------------|-------------|-------------------|
|           |                | Gene usage         | HCDR3 AA sequence         | Gene usage  | LCDR3 AA sequence |
| PVI.V5-1  | IgG1           | VH3-23 DH5-18 JH4  | CAPHRGQLWFDYW             | VK3-20 JK4  | CQQYGSSPPTF       |
| PVI.V5-2  | IgG1           | VH3-21 DH2-2 JH4   | CARDLKLSPAAIGWDYFDYW      | VK3-15 JK2  | CQQYNNWPRSF       |
| PVI.V5-3  | IgG1           | VH3-7 DH6-13 JH4   | CAIFGAAGTDYW              | VL3-16 JL3  | CLSADSSGTYWVF     |
| PVI.V5-4  | IgG1           | VH3-30 DH3-22 JH4  | CARENYYDSSGYSYFDYW        | VK3-20 JK2  | CQQYGSSPMCSF      |
| PVI.V5-5  | IgA1           | VH1-69 DH5-24 JH4  | CARDFGREWLQYFYFDCW        | VK3-20 JK4  | CQQYGSSPTF        |
| PVI.V5-6  | IgG1           | VH3-7 DH3-3 JH4    | CARDNDFWSGYLYFDYW         | VL3-10 JL2  | CYSTDSSGNHRGVF    |
| PVI.V6-1  | IgG1           | VH3-30 DH6-19 JH4  | CARGAVAGQHSFDNW           | VK2-30 JK4  | CMQGTHWPPPTF      |
| PVI.V6-2  | IgG1           | VH3-33 DH6-13 JH4  | CARDKRGSSSWLDQYFDYW       | VL3-21 JL2  | CQVWDSSTDHVVF     |
| PVI.V6-3  | IgG1           | VH4-31 DH3-22 JH5  | CARDMISGRGLFDPW           | VK1-33 JK2  | CQQYDNLPTF        |
| PVI.V6-4  | IgG1           | VH1-69 DH4-17 JH3  | CARGNYDYGDYLLKGSADFIDW    | VK4-1 JK2   | CQQYYSTPPNTF      |
| PVI.V6-5  | IgG1           | VH3-30 DH3-10 JH4  | CAKDGGYYYGSGSYPYFDYW      | VK2D-29 JK4 | CMQSIQLPLTF       |
| PVI.V6-6  | IgG1           | VH4-31 DH3-10 JH6  | CASEKFLWGQGYGMDVW         | VL2-14 JL2  | CSSYTSSSTLVF      |
| PVI.V6-7  | IgG1           | VH4-39 DH3-22 JH4  | CATQSDYDSSGLEFDYW         | VL2-14 JL3  | CSSYTSSSSWVF      |
| PVI.V6-8  | IgG1           | VH4-31 DH3-22 JH3  | CARGREEPIVVTFDAFDIW       | VK3-11 JK2  | CQQRSNWPPMYTF     |
| PVI.V6-9  | IgG1           | VH3-30 DH2-15 JH4  | CAKSGYPYCGGGTCYSGWFDYW    | VK1-33 JK2  | CQRYDNPPYTF       |
| PVI.V6-10 | IgG1           | VH1-2 DH6-19 JH6   | CAREIAVAGNDYSYGLDVW       | VK3-20 JK4  | CQQYGSSLLTF       |
| PVI.V6-11 | IgG1           | VH1-46 DH6-19 JH6  | CASQSHWQWLGGGDSYGMVW      | VK1-9 JK2   | CQQLNSYPYTF       |
| PVI.V6-12 | IgG1           | VH5-51 DH1-26 JH4  | CARRFGSYPYFDYW            | VL3-21 JL1  | CQVWDSNSDLYVF     |
| PVI.V6-13 | IgG1           | VH3-30 DH5-18 JH4  | CAKAGYSYAYGDYFDYW         | VK1-33 JK3  | CQHYDNLPPAVTF     |
| PVI.V6-14 | IgG1           | VH4-39 DH3-10 JH4  | CARCRPEYFSGSYLDFDYW       | VK1-12 JK4  | CQQANSFPLTF       |
| PVI.V6-15 | IgG1           | VH3-30 DH5-18 JH4  | CAKDWGWIQLWGLDYW          | VL2-18 JL3  | CSSYTSSSTWVF      |
| PVI.V3-1  | IgG1           | VH4-4 DH1-26 JH4   | CVSRGVGATREKDYW           | VK3-15 JK4  | CQQYNNWPPDLTF     |
| PVI.V3-2  | IgG1           | VH4-39 DH3-10 JH4  | CASLDYYGSGSGPYFDYW        | VK3-11 JK4  | CQQRSNWLTF        |
| PVI.V3-3  | IgG3           | VH3-33 DH6-19 JH4  | CASDSSGWYFDYW             | VL3-9 JL2   | CQVWDSSTVVF       |
| PVI.V3-4  | IgG1           | VH3-21 DH2-21 JH3  | CAVTLTPTYCGGEWCAFDIW      | VK3-15 JK2  | CQQYNNWPPYTF      |
| PVI.V3-5  | IgG1           | VH1-69 DH3-22 JH4  | CARNYYDSSGSQGMVW          | VK3-11 JK4  | CQQRSNWPPVLTF     |
| PVI.V3-6  | IgA1           | VH3-66 DH3-3 JH4   | CARHLGVVI <sup>1</sup>    | VK4-1 JK1   | CQQYYSTLWTF       |
| PVI.V3-7  | IgG3           | VH4-39 DH1-26 JH4  | CAKPSGSYLGFDYW            | VK1-39 JK3  | CQQSYSTPPTF       |
| PVI.V3-8  | IgG1           | VH4-38 DH3-3 JH4   | CARSDFSVRVGFDCW           | VK4-1 JK2   | CQQSYTTNTF        |
| PVI.V3-9  | IgG1           | VH3-53 DH3-16 JH6  | CARDLMEGGGMDVW            | VK3-20 JK1  | CQQYGSSLGTF       |
| PVI.V3-10 | IgG1           | VH4-34 DH3-22 JH4  | CARSQPLLWSSGYCCDYW        | VL2-11 JL2  | CCSYAGSYTLVF      |
| PVI.V3-11 | IgG1           | VH3-64D DH4-11 JH4 | CVRGPTVTTENDFDSW          | VK2-30 JK2  | CMQGTHSYTF        |
| PVI.V3-12 | IgG2           | VH1-46 DH5-24 JH4  | CASDPNRDGLALDSW           | VK3-20 JK2  | CQQYGTSPLYTF      |
| PVI.V3-13 | IgG1           | VH1-69 DH1-14 JH4  | CARDRYHGSPVDYW            | VK3-11 JK4  | CQQRSNWPPSLTF     |
| PVI.V3-14 | IgG1           | VH4-31 DH5-12 JH4  | CARARYSGSARGPPKQYFDYW     | VK3-20 JK1  | CQHLVTF           |
| PVI.V3-15 | IgG1           | VH3-21 DH3-3 JH3   | CARDGGRGYDFWSGYYIGAFDIW   | VK3-15 JK4  | CQQYNDWPPPLTF     |
| PVI.V3-16 | IgG1           | VH3-33 DH2-15 JH6  | CARGLGWDIVVVVSGEMDGMVW    | VL1-40 JL1  | CQSYDSSLSGPYVF    |
| PVI.V3-17 | IgA1           | VH3-20 DH2-2 JH4   | CARGESSDYW                | VK3-20 JK1  | CQQYGSSPKTF       |
| PVI.V3-18 | IgG1           | VH3-30 DH2-15 JH4  | CAKASGLYCSGGNCLVADFIDW    | VL1-39 JL4  | CQQSYSTPLSF       |
| PVI.V3-19 | IgG1           | VH5-51 DH6-19 JH6  | CARRNTSAQYSSGWYVHYYYGMDVW | VK2-28 JK3  | CMQALQTPGFTF      |
| PVI.V3-20 | IgG1           | VH3-30 DH3-3 JH6   | CAKDQLGAIFAHYYYGMDVW      | VL1-40 JL1  | CQSYDSSLSGYVF     |
| PVI.V3-21 | IgG1           | VH5-51 DH5-24 JH4  | CAKLSRDAYRGPFDYW          | VL6-57 JL2  | CQSYDSSNPVVF      |

<sup>1</sup>Indicates absence of the W118 residue from the junction of the CDR3.